The Time-Invariant Polynomial Model of Fixed-Frequency PWM DC–DC Converter Applying Normalized Coordinate Transformation

Yuan Chen, Bo Zhang, *Senior Member, IEEE*, Fan Xie, *Member, IEEE*, Dongyuan Qiu, *Member, IEEE*, and Yanfeng Chen, *Member, IEEE*

***Abstract*—In this article, a time-invariant polynomial model of fixed-frequency pulsewidth modulation dc–dc converter is proposed. Through normalized coordinate transformation, the time-varying model of the converter is transferred into a time-invariant model, whose state matrix and input matrix are obtained by the addition and multiplication of matrices simply and expressed by the polynomial of duty cycle concisely. The proposed model has the following advantages. Compared with the state-space average (SSA) model, the ripple of the state vector and the switching period are considered, thereby improving the accuracy. Contrary to other time-invariant models, the state matrix and input matrix instead of the state vector are expanded into series. Therefore, neither the number of state vectors nor the order of the matrices increases, and the proposed model has a simple structure similar to the SSA model. In addition, as a time-invariant polynomial model, the calculation and analysis of the proposed model are much simpler than the time-variant exact model. In order to prove the above advantages of the proposed model, the general expression of the proposed model is derived and the proposed model is compared with other models. These analyses and comparisons are verified through the simulation and experimental results.**

***Index Terms*—Coordinate transformation, normalization, polynomial models, pulsewdith modulation (PWM) dc–dc converters, time-invariant model.**

I. Introduction

NOWADAYS, pulsewidth modulation (PWM) dc–dc converters are an important part of power electronics systems, such as renewable energy generation systems and hybrid electric vehicle drive systems [1]. However, due to the time-varying characteristics of the PWM dc–dc converter, it is difficult to accurately model it.

To solve this problem, the state-space averaging (SSA) model is proposed. It is a simple time-invariant model, which can be analyzed and calculated easily [2]–[5]. Mathematically, the SSA model reflects the extreme situation of the PWM dc–dc converter when the switching period T approaches 0. Therefore, when the switching frequency is high, the SSA model is accurate. But when the switching frequency decreases, the error of the SSA model increases. Besides, the ripple of state vector is ignored in the SSA model as well. In response to these problems, several improved models were proposed, which can be divided into time-invariant models and time-variant models.

Time-invariant models mainly include the generalized state-space averaging (GSSA) model, multifrequency averaging (MFA) model, and Krylov–Bogoliubov–Mitropolsky (KBM) model. In the GSSA model [6]–[11] and the MFA model [12]–[14], the state vector is expanded into the Fourier series, and the harmonic balance method is used to generate the extended state matrix and input matrix. When more harmonics are considered, the error of the GSSA model and the MFA model will decrease, but the complexity will increase simultaneously. For example, when the mth harmonic is considered in the model, the order of state vectors and matrices should be $2m+1$ times larger. In the KBM model [15]–[18], the switching period T is regarded as the small parameter of the general KBM method, and the state vector is expanded into the Taylor series, whose terms are calculated successively. However, the KBM model regards the solution of the SSA model as the zero-order term in the Taylor series. When the switching frequency is low, the SSA model cannot accurately reflect the average behavior of the converter, and the error of the KBM model is also relatively large. In summary, the state vector expansion improves the accuracy of the existing time-invariant models. But when the accuracy increases, the model becomes more and more complex.

Time-variant models mainly include Floquet model and discrete-time model. In the Floquet model [19], the PWM converter is analyzed by Floquet theory. However, the Floquet theory is mainly used to analyze systems without input. Even if Floquet transformation is used, the input matrix of the PWM converter is still time varying. In the discrete-time model [20]–[24], the PWM converter is modeled by the time-varying equation, which is an exact model. However, compared with time-invariant models, the analysis and calculation of the time-variant models are generally more difficult. The complexity of the time-variant models limits their application.

Manuscript received December 9, 2020; revised March 18, 2021; accepted April 28, 2021. Date of publication May 10, 2021; date of current version July 30, 2021. This work was supported by the National Key Research and Development Program of China under Grant 2018YFB0905804. Recommended for publication by Associate Editor F. W. Fuchs. *(Corresponding author: Bo Zhang.)*

The authors are with the School of Electric Power, South China University of Technology, Guangzhou 510640, China (e-mail: yuanchensd@163.com; epbzhang@scut.edu.cn; epfxie@scut.edu.cn; epdyqiu@scut.edu.cn; eeyf chen@scut.edu.cn).

Color versions of one or more figures in this article are available at https://doi.org/10.1109/TPEL.2021.3078456.

Digital Object Identifier 10.1109/TPEL.2021.3078456

This article presents a time-invariant polynomial model of fixed-frequency PWM dc–dc converter. Using normalized coordinate transformation, the time-varying model of the converter is transferred into a time-invariant model, whose state matrix and input matrix are obtained by the addition and multiplication of matrices simply and expressed by the polynomial of duty cycle concisely. The advantages of the proposed model are summarized as follows.

1) Contrary to the SSA model, the ripple of state vector and the switching period of converter are considered in the proposed model. Therefore, the proposed model can provide the accurate ripples and more accurate average value of state vectors. And the proposed model can be used to analyze the influence of switching period and carrier on the stability of converter.
2) Compared with other time-invariant models, the state matrix and input matrix instead of the state vector are expanded into series. Therefore, the order of the state matrix and the input matrix in the proposed model is not increased, which simplifies the analysis and calculation. In addition, the state matrix and input matrix of the proposed model can be obtained by matrix addition and multiplication operations simply, and no other complex matrix operations are required in the final formula.
3) The Floquet model and the discrete-time model are both time-variant models, whose calculation and analysis are mathematically complex. However, the proposed mode is a time-invariant polynomial model, whose state matrix and input matrix can be expressed concisely with duty cycle polynomials. Therefore, the proposed model is much easier to be calculated and analyzed.

The rest of this article is structured as follows. In Section II, the principles of the proposed model are introduced. In Section III, the proposed model is compared with other time-invariant models. In Section IV, the simulation and experimental results of the basic converters ensure the correctness of the theoretical analysis and comparison. Finally, Section V presents the conclusion of this article.

II. Principles of the Proposed Model

In this section, the principles of the proposed model are explained. First, the PWM dc–dc converter is modeled with time-variant models with changing state matrices and input matrices. Then, the following coordinate transformation is used to normalize the values of state matrix and input matrix:

$$\mathbf{x}(t) = \mathbf{S}(t)\mathbf{x}^*(t) + \mathbf{P}(t)V_{\text{in}}(t) \tag{1}$$

where $\mathbf{x}(t)$ is the state vector in the original time-variant model, $\mathbf{x}^*(t)$ is the normalized state vector in the proposed time-invariant model, $V_{\text{in}}(t)$ is the input voltage, and $\mathbf{S}(t)$ and $\mathbf{P}(t)$ are the normalization transformation coefficients.

Finally, the normalized state vector is obtained in the following time-invariant model:

$$\dot{\mathbf{x}}^*(t) = \mathbf{A}^*\mathbf{x}^*(t) + \mathbf{B}^*V_{\text{in}}(t) \tag{2}$$

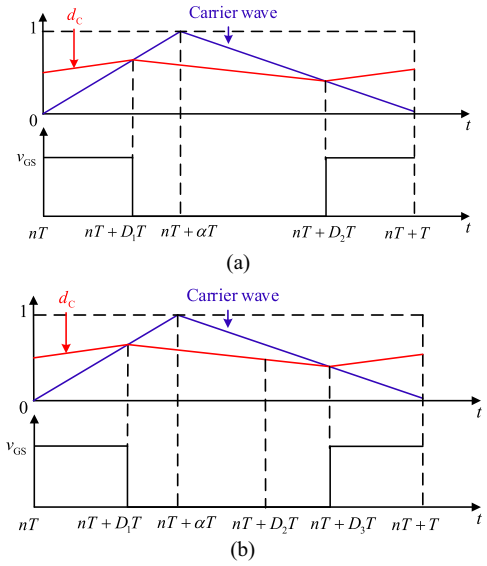

Fig. 1. Output of controller, carrier wave, and drive signal. (a) CCM. (b) DCM.

where $\mathbf{A}^*$ and $\mathbf{B}^*$ are the state matrix and input matrix of the proposed model, respectively, which will be calculated together with $\mathbf{S}(t)$ and $\mathbf{P}(t)$ later in this section.

A. Open-Loop Case

The relationship among the modulation signal d_C, carrier wave, and drive signal v_{GS} of PWM dc–dc converter is shown in Fig. 1, where T is the switching period, n is the number of switching periods, and $n = \text{INT}(t/T)$. The shape of the carrier wave is decided by the coefficient α. When α is 1, the carrier is the right-aligned carrier. When α is 0, the carrier is the left-aligned carrier. And when α is 0.5, the carrier is the center-aligned carrier.

The PWM dc–dc converters can be expressed with time-varying models. In the time interval $[nT+D_{k-1}T, nT+ D_kT)$, the converter is in interval k and

$$D_k = \sum_{i=1}^{k} d_{Si} \tag{3}$$

where d_{Si} is the duty cycle of interval i.

The state-space equation of interval k can be expressed as

$$\begin{cases} \dot{\mathbf{x}}(t) = \mathbf{A}_k\mathbf{x}(t) + \mathbf{B}_kV_{\text{in}}(t) \\ v_{\text{o}} = \mathbf{C}_k\mathbf{x}(t) \end{cases} \tag{4}$$

where $\mathbf{A}_k$ is the state matrix, $\mathbf{B}_k$ is the input matrix, and $\mathbf{C}_k$ is the output matrix.

When the converter operates in continuous conductive mode (CCM), intervals 1 and 3 correspond to mode 1, and interval 2 corresponds to mode 2. When the converter operates in discontinuous conductive mode (DCM), intervals 1 and 4 correspond to mode 1, interval 2 corresponds to mode 2, and interval 3 corresponds to mode 3.

Substituting (1) and (2) into (4), it is obtained that

$$[\dot{\mathbf{S}}(t) + \mathbf{S}(t)\mathbf{A}^* - \mathbf{A}_k\mathbf{S}(t)]\mathbf{x}^*(t)$$

$$+[\dot{\mathbf{P}}(t)+\mathbf{S}(t)\mathbf{B}^*-\mathbf{A}_k\mathbf{P}(t)-\mathbf{B}_k]V_{\rm in}(t)=0. \tag{5}$$

In order to make (5) constant for any $\mathbf{x}^*(t)$ and $V_{\rm in}(t)$, their coefficients should be zero. Therefore, the normalization transformation coefficients should satisfy

$$\dot{\mathbf{S}}(t)=\mathbf{A}_k\mathbf{S}(t)-\mathbf{S}(t)\mathbf{A}^* \tag{6}$$

$$\dot{\mathbf{P}}(t)=\mathbf{A}_k\mathbf{P}(t)-\mathbf{S}(t)\mathbf{B}^*+\mathbf{B}_k. \tag{7}$$

Since there is no boundary condition, the number of solutions of (6) and (7) is infinite [25]. In the time interval [nT, nT+T), the general solution is expressed as

$$\mathbf{S}(t)=e^{\mathbf{A}_k(t-nT)}\mathbf{O}e^{-\mathbf{A}^*(t-nT)} \tag{8}$$

$$\mathbf{P}(t)=(e^{\mathbf{A}_k(t-nT)}\mathbf{L}-\mathbf{E})\mathbf{A}_k^{-1}\mathbf{B}_k - \mathbf{S}(t)(e^{\mathbf{A}^*(t-nT)}-\mathbf{E})\mathbf{A}^{*-1}\mathbf{B}^* \tag{9}$$

where $\mathbf{E}$ is the identity matrix, and $\mathbf{O}$ and $\mathbf{L}$ are the undetermined coefficients determined by the boundary conditions. In the interval k, the $\mathbf{O}$ is $\mathbf{O}_k$, and the $\mathbf{L}$ is $\mathbf{L}_k$. They are obtained by the continuity of $\mathbf{S}(t)$ and $\mathbf{P}(t)$ at the time point nT+$D_{k-1}T$

$$\begin{cases}\mathbf{O}_{k+1}= e^{-\mathbf{A}_{k+1}D_kT}e^{\mathbf{A}_kD_kT}\mathbf{O}_k\\ \mathbf{L}_{k+1}= e^{-\mathbf{A}_{k+1}D_kT}[\mathbf{E}+(e^{\mathbf{A}_kD_kT}\mathbf{L}_k-\mathbf{E})\\ \qquad\times\mathbf{A}_k^{-1}\mathbf{B}_k\mathbf{B}_{k+1}^{-1}\mathbf{A}_{k+1}].\end{cases} \tag{10}$$

As shown in (8)–(10), the $\mathbf{S}(t)$ and $\mathbf{P}(t)$ are determined by $\mathbf{O}_1$, $\mathbf{L}_1$, $\mathbf{A}^*$, and $\mathbf{B}^*$. In order to simplify the application of the model, the $\mathbf{S}(t)$ and $\mathbf{P}(t)$ should be continuous periodic functions with period T. Therefore, the values of $\mathbf{A}^*$ and $\mathbf{B}^*$ are selected by the following equations:

$$\begin{cases}\lim\limits_{t\to(nT)^+}\mathbf{S}(t)=\lim\limits_{t\to(nT)^-}\mathbf{S}(t)=\lim\limits_{t\to(nT+T)^-}\mathbf{S}(t)\\ \lim\limits_{t\to(nT)^+}\mathbf{P}(t)=\lim\limits_{t\to(nT)^-}\mathbf{P}(t)=\lim\limits_{t\to(nT+T)^-}\mathbf{P}(t).\end{cases} \tag{11}$$

Substituting (8)–(10) into (11), the $\mathbf{A}^*$ and $\mathbf{B}^*$ should satisfy the following equations:

$$e^{\mathbf{A}^*T}=\mathbf{O}_1^{-1}\prod_{k=1}^{N}e^{\mathbf{A}_kd_kT}\mathbf{O}_1 \tag{12}$$

$$\mathbf{B}^*=\mathbf{A}^*(e^{\mathbf{A}^*T}-\mathbf{E})^{-1}\mathbf{O}_1^{-1} \times[(e^{\mathbf{A}_NT}\mathbf{L}_N-\mathbf{E})\mathbf{A}_N^{-1}\mathbf{B}_N-(\mathbf{L}_1-\mathbf{E})\mathbf{A}_1^{-1}\mathbf{B}_1]. \tag{13}$$

Through the coefficient matching method, the $\mathbf{A}^*$ and $\mathbf{B}^*$ can be concisely expressed by duty cycle polynomials. Using different $\mathbf{O}_1$ and $\mathbf{L}_1$, the expression of $\mathbf{A}^*$, $\mathbf{B}^*$, $\mathbf{S}(t)$, and $\mathbf{P}(t)$ is different. To make the model easier to use, the $\mathbf{O}_1$ and $\mathbf{L}_1$ should be chosen to eliminate the terms in $\mathbf{A}^*$ and $\mathbf{B}^*$. In order to eliminate the influence of α in $\mathbf{A}^*$ and $\mathbf{B}^*$, take $\mathbf{O}_1$ and $\mathbf{L}_1$ as

$$\mathbf{O}_1=\mathbf{L}_1=e^{(0.5-\alpha)\mathbf{A}_1d_1T}. \tag{14}$$

And the expressions of $\mathbf{A}^*$ and $\mathbf{B}^*$ are

$$\mathbf{A}^*=\sum_{p=0}^{\infty}\mathbf{A}_p^*T^p=\sum_{p=0}^{m}\mathbf{A}_p^*T^p+O(T^{m+1}) \tag{15}$$

$$\mathbf{B}^*=\sum_{p=0}^{\infty}\mathbf{B}_p^*T^p=\sum_{p=0}^{m}\mathbf{B}_p^*T^p+O(T^{m+1}). \tag{16}$$

For the converter that operates in DCM, the iterative formula of $\mathbf{A}_p^*$ is

$$\mathbf{A}_0^*=d_1\mathbf{A}_1+d_2\mathbf{A}_2+d_3\mathbf{A}_3 \tag{17}$$

$$\mathbf{A}_p^*=\sum_{i+j+m+n=p+1}\frac{d_1^{m+n}d_2^id_3^j\mathbf{A}_1^m\mathbf{A}_2^i\mathbf{A}_3^j\mathbf{A}_1^n}{2^{m+n}m!n!i!j!}-\sum_{r=0}^{p-1}\frac{\sum\mathbf{Y}}{(r+2)!} \tag{18}$$

where the matrix $\mathbf{Y}$ satisfies

$$\mathbf{Y}\in\mathbf{Y}^*(p,r)=\{\,\mathbf{Y}|\ \mathbf{Y}=\prod_{j=0}^{r+1}\mathbf{A}_{n_j}^*,\ \textstyle\sum_{j=0}^{r+1}n_j=p-1-r\,\}. \tag{19}$$

For the converter with CCM, the $\mathbf{A}_p^*$ can be obtained by substituting $d_3=0$ into (17)–(19).

The formula of $\mathbf{B}_p^*$ is similar to that of $\mathbf{A}_p^*$. If the formula of $\mathbf{A}_p^*$ obtained by (17) and (18) is expressed as

$$\mathbf{A}_p^*=\begin{cases}\mathbf{F}_{p1}^*\mathbf{A}_1+\mathbf{F}_{p2}^*\mathbf{A}_2 & ,\ \text{CCM}\\ \mathbf{F}_{p1}^*\mathbf{A}_1+\mathbf{F}_{p2}^*\mathbf{A}_2+\mathbf{F}_{p3}^*\mathbf{A}_3 & ,\ \text{DCM}\end{cases} \tag{20}$$

the formula of $\mathbf{B}_p^*$ can be expressed as

$$\mathbf{B}_p^*=\begin{cases}\mathbf{F}_{p1}^*\mathbf{B}_1+\mathbf{F}_{p2}^*\mathbf{B}_2 & ,\ \text{CCM}\\ \mathbf{F}_{p1}^*\mathbf{B}_1+\mathbf{F}_{p2}^*\mathbf{B}_2+\mathbf{F}_{p3}^*\mathbf{B}_3 & ,\ \text{DCM.}\end{cases} \tag{21}$$

In short, the $\mathbf{B}_p^*$ is obtained by replacing the last $\mathbf{A}_1$, $\mathbf{A}_2$, and $\mathbf{A}_3$ in the product terms of the $\mathbf{A}_p^*$ with $\mathbf{B}_1$, $\mathbf{B}_2$, and $\mathbf{B}_3$, respectively. The proofs of (17)–(21) are shown in the appendix.

As shown in (17)–(21), the $\mathbf{A}_p^*$ and $\mathbf{B}_p^*$ are expressed by the duty cycle polynomials and the degree of the polynomials is p+1. In Section IV, the PWM dc–dc converter is expressed with the first three terms of $\mathbf{A}_p^*$ and $\mathbf{B}_p^*$. For the converter with DCM, the $\mathbf{B}_0{}^*$ is

$$\mathbf{B}_0^*=d_1\mathbf{B}_1+d_2\mathbf{B}_2+d_3\mathbf{B}_3 \tag{22}$$

the $\mathbf{A}_1{}^*$ and $\mathbf{B}_1{}^*$ are

$$\mathbf{A}_1^*=\frac{d_2d_3}{2}(\mathbf{A}_2\mathbf{A}_3-\mathbf{A}_3\mathbf{A}_2) \tag{23}$$

$$\mathbf{B}_1^*=\frac{d_2d_3}{2}(\mathbf{A}_2\mathbf{B}_3-\mathbf{A}_3\mathbf{B}_2) \tag{24}$$

and the $\mathbf{A}_2^*$ and $\mathbf{B}_2^*$ can be expressed as

$$\mathbf{A}_2^*=\left(\frac{d_1d_2^2}{12}\tilde{\mathbf{A}}_2^2-\frac{d_1^2d_2}{24}\tilde{\mathbf{A}}_2\mathbf{A}_1+\frac{d_1^2d_2}{12}\mathbf{A}_1\tilde{\mathbf{A}}_2\right)\mathbf{A}_1 +\left(\frac{d_1d_2^2}{12}\mathbf{A}_1\tilde{\mathbf{A}}_2-\frac{d_1^2d_2}{24}\mathbf{A}_1{}^2-\frac{d_1d_2^2}{6}\tilde{\mathbf{A}}_2\mathbf{A}_1\right)\tilde{\mathbf{A}}_2 -\frac{1}{6}\mathbf{A}_1^*(2d_3\mathbf{A}_3+d_2\mathbf{A}_2)-\frac{1}{6}(d_3\mathbf{A}_3+2d_2\mathbf{A}_2)\mathbf{A}_1^* \tag{25}$$

$$\mathbf{B}_2^*=\left(\frac{d_1d_2^2}{12}\tilde{\mathbf{A}}_2^2-\frac{d_1^2d_2}{24}\tilde{\mathbf{A}}_2\mathbf{A}_1+\frac{d_1^2d_2}{12}\mathbf{A}_1\tilde{\mathbf{A}}_2\right)\mathbf{B}_1$$

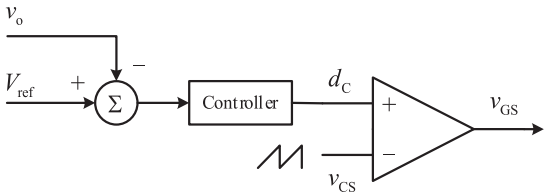

Fig. 2. Structure of controller in the PWM dc–dc converter.

$$+\left(\frac{d_1d_2^2}{12}\mathbf{A}_1\tilde{\mathbf{A}}_2-\frac{d_1^2d_2}{24}\mathbf{A}_1{}^2-\frac{d_1d_2^2}{6}\tilde{\mathbf{A}}_2\mathbf{A}_1\right)\tilde{\mathbf{B}}_2$$
$$-\frac{1}{6}\mathbf{A}_1^*(2d_3\mathbf{B}_3+d_2\mathbf{B}_2)-\frac{1}{6}(d_3\mathbf{A}_3+2d_2\mathbf{A}_2)\mathbf{B}_1^* \tag{26}$$

where

$$\tilde{\mathbf{A}}_2=\mathbf{A}_2+\frac{d_3}{d_2}\mathbf{A}_3,\quad \tilde{\mathbf{B}}_2=\mathbf{B}_2+\frac{d_3}{d_2}\mathbf{B}_3. \tag{27}$$

For the converter with CCM, the $\mathbf{A}_p^*$ and $\mathbf{B}_p^*$ can be obtained by substituting $d_3=0$ into (22)–(27). In this case, the $\mathbf{A}_1{}^*$ and $\mathbf{B}_1^*$ are both zero due to the usage of (14).

By calculating more $\mathbf{A}_p^*$ and $\mathbf{B}_p^*$ in (15) and (16), the accuracy of the proposed model can be improved. Increasing the order of the proposed model only increases the degree of the polynomials, and the order of the state vector and matrices does not increase.

When the converter operates in the open-loop case, the duty cycle d_1 is decided by the external controller. For the converter that operates in CCM, the duty cycle d_2 is

$$d_2=1-d_1. \tag{28}$$

For the converter that operates in DCM, the inductor current is 0 at time point $nT+D_2T$

$$i_{\rm L}(nT+D_2T)=0. \tag{29}$$

The relationship of d_1 and d_2 can be obtained by substituting (1) into (29). And the duty cycle d_3 is

$$d_3=1-d_1-d_2. \tag{30}$$

B. Closed-Loop Case

When the converter is in a closed-loop state, it is necessary to consider the influence of the controller's parameters and state vector on the duty cycle. The general structure of controller in the PWM dc–dc converter is shown in Fig. 2, where $V_{\rm ref}$ is the reference output voltage, $v_{\rm o}$ is the output voltage, $d_{\rm C}$ is the output of controller, $v_{\rm CS}$ is the carrier wave of the controller, and $v_{\rm GS}$ is the drive signal of the switch.

The linear controller is widely used in industrial application, which can be expressed by the state-space equation

$$\begin{cases}\dot{\mathbf{x}}_{\rm C}(t)=\mathbf{A}_{\rm C}\mathbf{x}_{\rm C}(t)+\mathbf{B}_{\rm C}(V_{\rm ref}-v_{\rm o})\\ d_{\rm C}(t)=\mathbf{C}_{\rm C}\mathbf{x}_{\rm C}(t)+\mathbf{D}_{\rm C}(V_{\rm ref}-v_{\rm o}).\end{cases} \tag{31}$$

In order to avoid repeated discussions, the converter with a linear controller is transferred into the same form of open-loop case. Substituting (31) into (4), in the time interval $[nT+D_{k-1}T, nT+D_kT)$, the converter with linear controller can be expressed as

$$\begin{cases}\dot{\mathbf{x}}_{{\rm au}}(t)=\mathbf{A}_{{\rm au}k}\mathbf{x}_{{\rm au}}(t)+\mathbf{B}_{{\rm au}k}\mathbf{u}(t)\\ d_{\rm C}(t)=\mathbf{C}_{{\rm au}k}\mathbf{x}_{{\rm au}}(t)+\mathbf{D}_{\rm C}V_{\rm ref}\end{cases} \tag{32}$$

where the $\mathbf{x}_{{\rm au}}(t)$ is the augmented state vector, $\mathbf{u}$ is the augmented input vector, $\mathbf{A}_{{\rm au}k}$ is the augmented state matrix, $\mathbf{B}_{{\rm au}k}$ is the augmented input matrix, and $\mathbf{C}_{{\rm au}k}$ is the augmented output matrix. Their values are listed in Table I.

TABLE I
AUGMENTED MATRICES FOR CONVERTER WITH CONTROLLER

Item	Original	Augmented
State vector	$\mathbf{x}(t)$	$\mathbf{x}_{\rm au}(t)=[\mathbf{x}(t)^{\rm T}\quad \mathbf{x}_{\rm C}(t)^{\rm T}]^{\rm T}$
Input vector	$V_{\rm in}(t)$	$\mathbf{u}(t)=[V_{\rm in}(t)\quad V_{\rm ref}(t)]^{\rm T}$
State matrixes	$\mathbf{A}_k$	$\mathbf{A}_{{\rm au}k}=\begin{bmatrix}\mathbf{A}_k & 0\\ -\mathbf{B}_{\rm C}\mathbf{C}_k & \mathbf{A}_{\rm C}\end{bmatrix}$
Input matrixes	$\mathbf{B}_k$	$\mathbf{B}_{{\rm au}k}=\begin{bmatrix}\mathbf{B}_k & 0\\ 0 & \mathbf{B}_{\rm C}\end{bmatrix}$
Output matrixes	$\mathbf{C}_k$	$\mathbf{C}_{{\rm au}k}=\begin{bmatrix}-\mathbf{D}_{\rm C}\mathbf{C}_k & \mathbf{C}_{\rm C}\end{bmatrix}$

As (32) has the same form of (4), the discussion result of (4) can be used for (32) as well. The normalized coordinate transformation is

$$\mathbf{x}_{{\rm au}}(t)=\mathbf{S}_{{\rm au}}(t)\mathbf{x}_{{\rm au}}{}^*(t)+\mathbf{P}_{{\rm au}}(t)\mathbf{u}(t) \tag{33}$$

where $\mathbf{x}_{{\rm au}}{}^*(t)$ is the state vector of the following time-invariant model

$$\dot{\mathbf{x}}_{{\rm au}}^*(t)=\mathbf{A}_{{\rm au}}{}^*\mathbf{x}_{{\rm au}}{}^*(t)+\mathbf{B}_{{\rm au}}{}^*\mathbf{u}(t). \tag{34}$$

The values of $\mathbf{S}_{{\rm au}}(t)$, $\mathbf{P}_{{\rm au}}(t)$, $\mathbf{A}_{{\rm au}}{}^*$, and $\mathbf{B}_{{\rm au}}{}^*$ can be calculated by replacing the original vectors and matrices with the corresponding augmented vectors and matrices, as given in Table I.

Compared with the open-loop case, the value of d_1 is decided by the state vector of the converter in the closed-loop case. As shown in Fig. 1, the relationship between $d_1(t)$ and $d_{\rm C}(t)$ can be expressed as

$$d_1(t)=\alpha d_{\rm C}(nT+\alpha d_1T)+(1-\alpha)d_{\rm C}(nT+T-(1-\alpha)d_1T). \tag{35}$$

Substituting (32) and (33) into (35) and remaining the linear term of switching period T, when the converter operates in CCM, (35) can be simplified as

$$d_1(t)\approx\alpha\mathbf{C}_{{\rm au}1}[(\mathbf{E}+0.5\mathbf{A}_{{\rm au}1}d_1T)\mathbf{x}_{{\rm au}}{}^*$$
$$+0.5\mathbf{B}_{{\rm au}1}d_1T\mathbf{u}]+\mathbf{D}_{\rm C}V_{\rm ref}+(1-\alpha)\mathbf{C}_{{\rm au}2}$$
$$\times[(\mathbf{E}-0.5\mathbf{A}_{{\rm au}1}d_1T)\mathbf{x}_{{\rm au}}{}^*-0.5\mathbf{B}_{{\rm au}1}d_1T\mathbf{u}]. \tag{36}$$

Then, the duty cycle $d_1(t)$ can be expressed by $\mathbf{x}_{{\rm au}}{}^*(t)$ explicitly.

$$d_1(t)=\frac{[\alpha\mathbf{C}_{{\rm au}1}+(1-\alpha)\mathbf{C}_{{\rm au}2}]\mathbf{x}_{{\rm au}}{}^*(t)+\mathbf{D}_{\rm C}V_{\rm ref}}{1-0.5T[\alpha\mathbf{C}_{{\rm au}1}-(1-\alpha)\mathbf{C}_{{\rm au}2}][\mathbf{A}_{{\rm au}1}\mathbf{x}_{{\rm au}}{}^*(t)+\mathbf{B}_{{\rm au}1}\mathbf{u}(t)]}. \tag{37}$$

When the converter operates in DCM, the $\mathbf{C}_{\mathrm{au2}}$ in (36) and (37) should be replaced by $\mathbf{C}_{\mathrm{au3}}$.

In summary, the expressions of $\mathbf{x}_{\mathrm{au}}{}^{*}(t)$ and $d_1(t)$ contain (34) and (37), which make up a standard system of ordinary differential equations. After obtaining $\mathbf{x}_{\mathrm{au}}{}^{*}(t)$ and $d_1(t)$, the value of $d_2(t)$, $d_3(t)$, $\mathbf{S}_{\mathrm{au}}(t)$, and $\mathbf{P}_{\mathrm{au}}(t)$ can be obtained as well. Finally, the value of $\mathbf{x}_{\mathrm{au}}(t)$ is obtained by (33).

The discussion of nonlinear controller is more complex than linear controller. There are dozens of control methods, which cannot be discussed one-by-one. Besides, the main purpose of this article is to propose a modeling method of converter rather than a general analysis method of nonlinear controller. Therefore, this article mainly focuses on the interface between the converter modeled by the proposed method and controller.

Generally, the nonlinear controller can be expressed by the following differential equation:

$$\begin{cases} \dot{\mathbf{x}}_{\mathrm{C}}(t) = \mathbf{F}_{\mathrm{C}}(\mathbf{x}_{\mathrm{C}}, V_{\mathrm{ref}} - v_{\mathrm{o}}) \\ d_{\mathrm{C}}(t) = \mathbf{G}_{\mathrm{C}}(\mathbf{x}_{\mathrm{C}}, V_{\mathrm{ref}} - v_{\mathrm{o}}). \end{cases} \tag{38}$$

To eliminate intermediate variables, the v_{o} in (38) should be represented by $\mathbf{x}^{*}(t)$, and the $d_1(t)$ should be represented by $d_{\mathrm{C}}(t)$. Substituting (1) into (3), the v_{o} can be expressed as

$$v_{\mathrm{o}} = \mathbf{C}_k[\mathbf{S}(t)\mathbf{x}^{*}(t) + \mathbf{P}(t)V_{\mathrm{in}}(t)]. \tag{39}$$

The relationship between $d_1(t)$ and $d_{\mathrm{C}}(t)$ is expressed by (35).

The general form of the converter with nonlinear closed-loop controller can be expressed by (1), (2), (35), (38), and (39).

C. Frequency-Domain Analysis

The frequency-domain analysis is a general tool of linear-controller design. As an analytical model, the proposed model can be used in the frequency-domain analysis as the other time-invariant model. To simplify the analysis, it is assumed that the converter operates in the CCM state. Using small-signal analysis, (34) can be expressed as

$$\frac{d\hat{\mathbf{x}}^{*}_{\mathrm{au}}}{dt} = \bar{\mathbf{A}}^{*}_{\mathrm{au}}\hat{\mathbf{x}}^{*}_{\mathrm{au}} + \bar{\mathbf{B}}^{*}_{\mathrm{au}}\hat{\mathbf{u}} + \left[\frac{\partial \mathbf{A}_{\mathrm{au}}{}^{*}}{\partial d_1}\bar{\mathbf{x}}^{*}_{\mathrm{au}} + \frac{\partial \mathbf{B}_{\mathrm{au}}{}^{*}}{\partial d_1}\bar{\mathbf{u}}\right]\hat{d}_1 \tag{40}$$

where $\hat{\mathbf{x}}_{\mathrm{au}}$, $\hat{\mathbf{u}}$, and $\hat{d}_1$ are the small disturbances of the augmented state vector, augmented input vector, and duty cycle d_1, respectively, and $\bar{\mathbf{x}}_{\mathrm{au}}$, $\bar{\mathbf{u}}$, $\bar{\mathbf{A}}_{\mathrm{au}}$, and $\bar{\mathbf{B}}_{\mathrm{au}}$ are the steady-state values of the augmented state vector, augmented input vector, augmented state matrix, and augmented input matrix, respectively.

Using Laplace transform, (40) can be expressed as

$$\frac{\hat{\mathbf{x}}^{*}_{\mathrm{au}}(s)}{\hat{d}_1(s)} = (s\mathbf{E} - \bar{\mathbf{A}}_{\mathrm{au}})^{-1}\left[\frac{\partial \mathbf{A}_{\mathrm{au}}{}^{*}}{\partial d_1}\bar{\mathbf{x}}^{*}_{\mathrm{au}} + \frac{\partial \mathbf{B}_{\mathrm{au}}{}^{*}}{\partial d_1}\bar{\mathbf{u}}\right]\Bigg|_{\hat{\mathbf{u}}=0}. \tag{41}$$

The transfer function between $\hat{\mathbf{x}}_{\mathrm{au}}$ and $\hat{d}_1$ can be obtained by substituting (15)–(27) into (41).

Using small-signal analysis and Laplace transform, the $\hat{d}_1(s)$ can be expressed as

$$\begin{aligned} \hat{d}_1(s) &= \frac{(\mathbf{\Phi}_1 e^{-0.5\bar{d}_1 Ts} + \mathbf{\Phi}_2 e^{0.5\bar{d}_1 Ts})\hat{\mathbf{x}}^{*}_{\mathrm{au}}(s)}{1 - 0.5T(\mathbf{\Phi}_1 - \mathbf{\Phi}_2)(\mathbf{A}_{\mathrm{au1}}\bar{\mathbf{x}}^{*}_{\mathrm{au}} + \mathbf{B}_{\mathrm{au1}}\bar{\mathbf{u}})}\Bigg|_{\hat{\mathbf{u}}=0} \\ &\approx \frac{[(\mathbf{\Phi}_1 + \mathbf{\Phi}_2) - (\mathbf{\Phi}_1 - \mathbf{\Phi}_2)0.5\bar{d}_1 Ts]\hat{\mathbf{x}}^{*}_{\mathrm{au}}(s)}{1 - 0.5T(\mathbf{\Phi}_1 - \mathbf{\Phi}_2)(\mathbf{A}_{\mathrm{au1}}\bar{\mathbf{x}}^{*}_{\mathrm{au}} + \mathbf{B}_{\mathrm{au1}}\bar{\mathbf{u}})}\Bigg|_{\hat{\mathbf{u}}=0} \end{aligned} \tag{42}$$

where

$$\mathbf{\Phi}_1 = \alpha\mathbf{C}_{\mathrm{au1}}e^{0.5\mathbf{A}_{\mathrm{au1}}\bar{d}_1 T}, \quad \mathbf{\Phi}_2 = (1-\alpha)\mathbf{C}_{\mathrm{au2}}e^{-0.5\mathbf{A}_{\mathrm{au1}}\bar{d}_1 T}. \tag{43}$$

The proof of (42) is shown in the Appendix. The open-loop transfer function can be obtained by multiplying (41) with (42).

III. Comparison

In this section, other time-invariant models, including the SSA model, the GSSA model, the MFA model, and the KBM model, are analyzed and compared with the proposed model. These time-invariant models can be regarded as the low-order approximations of the proposed model. As these models mainly focus on the converter with CCM, the comparison focuses on the converter with CCM as well.

A. SSA and the Proposed Models

In the SSA model, the average value of state vector $\mathbf{x}_{\mathrm{ave}}(t)$ is obtained by

$$\begin{aligned} \dot{\mathbf{x}}_{\mathrm{ave}}(t) &= (\mathbf{A}_1 d_1 + \mathbf{A}_2 d_2)\mathbf{x}_{\mathrm{ave}}(t) + (\mathbf{B}_1 d_1 + \mathbf{B}_2 d_2)V_{\mathrm{in}}(t) \\ &= \mathbf{A}_{\mathrm{ave}}\mathbf{x}_{\mathrm{ave}}(t) + \mathbf{B}_{\mathrm{ave}}V_{\mathrm{in}}(t). \end{aligned} \tag{44}$$

In the proposed model, the $\mathbf{x}(t)$ is equal to $\mathbf{x}^{*}(t)$ when the switching period T approaches 0.

$$\begin{aligned} \lim_{T\to 0}\mathbf{x}(t) &= \lim_{T\to 0}\mathbf{S}(t)\lim_{T\to 0}\mathbf{x}^{*}(t) + \lim_{T\to 0}\mathbf{P}(t)V_{\mathrm{in}}(t) \\ &= \mathbf{E}\lim_{T\to 0}\mathbf{x}^{*}(t) + 0V_{\mathrm{in}}(t) \\ &= \lim_{T\to 0}\mathbf{x}^{*}(t). \end{aligned} \tag{45}$$

And, $\mathbf{A}^{*}$ and $\mathbf{B}^{*}$ obtained by (15) and (16) are

$$\begin{cases} \lim\limits_{T\to 0}\mathbf{A}^{*} = \mathbf{A}^{*}_0 = \mathbf{A}_1 d_1 + \mathbf{A}_2 d_2 = \mathbf{A}_{\mathrm{ave}} \\ \lim\limits_{T\to 0}\mathbf{B}^{*} = \mathbf{B}^{*}_0 = \mathbf{B}_1 d_1 + \mathbf{B}_2 d_2 = \mathbf{B}_{\mathrm{ave}}. \end{cases} \tag{46}$$

Therefore, the SSA model is the low-order approximation of the proposed model when the switching period is 0. Due to the performance limitations of actual switching devices, the switching period cannot be 0. When the switching period is not small enough to be regarded as 0, the accuracy of the proposed model is higher. Besides, the ripple of state vector can be calculated by $\mathbf{S}(t)$ and $\mathbf{P}(t)$, which is ignored in the SSA model as well.

B. KBM and the Proposed Models

In the KBM model, piecewise functions are used to express the ripple of the state vector. The standard form of the KBM model is

$$\dot{\mathbf{x}}(t) = \varepsilon\mathbf{F}(t, \mathbf{x}, V_{\mathrm{in}}),\ \varepsilon \ll 1\,. \tag{47}$$

And the state vector is expanded into the Taylor series of a small parameter ε.

$$\mathbf{x}(t) = \mathbf{z}(t) + \sum_{k=1}^{m} \varepsilon^k \boldsymbol{\psi}_k(t, \mathbf{z}, V_{\text{in}}) + O(\varepsilon^{m+1}) \tag{48}$$

$$\dot{\mathbf{z}}(t) = \sum_{k=1}^{m} \varepsilon^k \mathbf{G}_k(t, \mathbf{z}, V_{\text{in}}) + O(\varepsilon^{m+1}). \tag{49}$$

When the small parameter ε is the switching period T, the average state vector $\mathbf{z}(t)$ is the result of the SSA model [16], and the $\boldsymbol{\Psi}_k$ is the kth ripple of the KBM model

$$\begin{cases} \boldsymbol{\psi}_1(t, \mathbf{z}, V_{\text{in}}) = \int_0^t [\mathbf{F}(t, \mathbf{z}, V_{\text{in}}) - \mathbf{G}_1(\mathbf{z}, V_{\text{in}})]dt + \mathbf{h}_1(\mathbf{z}) \\ \boldsymbol{\psi}_k(t, \mathbf{z}, V_{\text{in}}) = \int_0^t [\mathbf{F}(t, \boldsymbol{\psi}_{k-1}, V_{\text{in}}) - \mathbf{G}_k(\mathbf{z}, V_{\text{in}})]dt + \mathbf{h}_k(\mathbf{z}) \end{cases} \tag{50}$$

where $\mathbf{h}_k$ is chosen so that the average value of $\boldsymbol{\Psi}_k$ is 0.

Since the average state vector $\mathbf{z}(t)$ is the result of the SSA model, the relationship between $\mathbf{z}(t)$ in the KBM model and the $\mathbf{x}^*(t)$ in the proposed model can be expressed as

$$\mathbf{z}(t) = \mathbf{x}_{\text{ave}}(t) = \lim_{T \to 0} \mathbf{x}^*(t). \tag{51}$$

And the relationship among $\boldsymbol{\Psi}(t)$, $\mathbf{S}(t)$, and $\mathbf{P}(t)$ is

$$\boldsymbol{\psi}_k(t, \mathbf{z}, V_{\text{in}}) = \mathbf{S}_k(t)\mathbf{z}(t) + \mathbf{P}_k(t)V_{\text{in}}(t) \tag{52}$$

where $\mathbf{S}_k(t)$ and $\mathbf{P}_k(t)$ are the coefficients in the Taylor series of $\mathbf{S}(t)$ and $\mathbf{P}(t)$, respectively, and

$$\begin{cases} \mathbf{S}(t) = \mathbf{E} + \sum_{k=1}^{m} \mathbf{S}_k(t)T^k + O(T^{m+1}) \\ \mathbf{P}(t) = \mathbf{E} + \sum_{k=1}^{m} \mathbf{P}_k(t)T^k + O(T^{m+1}). \end{cases} \tag{53}$$

Therefore, the KBM model is the low-order approximation of the proposed model, when the switching period T is regarded as 0 to obtain $\mathbf{x}^*(t)$ and high-order terms in the Taylor series of $\mathbf{S}(t)$ and $\mathbf{P}(t)$ are ignored. In addition, it is mathematically difficult to get the formula using (50). But $\mathbf{S}(t)$ and $\mathbf{P}(t)$ are represented by (8) and (9) directly.

C. GSSA, MFA, and the Proposed Models

In the GSSA and MFA models, the state-space equation of the converter is expressed by switching function $s(t)$.

$$\begin{aligned} \dot{\mathbf{x}}(t) = &[(\mathbf{A}_1 - \mathbf{A}_2)s(t) + \mathbf{A}_2]\mathbf{x}(t) \\ &+ [(\mathbf{B}_1 - \mathbf{B}_2)s(t) + \mathbf{B}_2]V_{\text{in}}(t). \end{aligned} \tag{54}$$

And, the state vector $\mathbf{x}(t)$ and switching function $s(t)$ are expanded into the Fourier series

$$\begin{cases} \mathbf{x}(t) = \mathbf{x}_0(t) + \sum_{k=1}^{m} [\mathbf{x}_{ak}(t)\sin(k\omega_s t) + \mathbf{x}_{bk}(t)\cos(k\omega_s t)] \\ s(t) = s_0 + \sum_{k=1}^{m} [s_{ak}\sin(k\omega_s t) + s_{bk}\cos(k\omega_s t)] \end{cases} \tag{55}$$

where ω_s is the switching angular frequency and m is the order of the GSSA and MFA model. Then, the expanded state matrix and input matrix are calculated by the harmonic balance method.

The state vector in the proposed model can be expressed by the Fourier series as well. As the $\mathbf{S}(t)$ and $\mathbf{P}(t)$ are periodic functions whose angular frequency is ω_s as well, the Fourier series of $\mathbf{S}(t)$ and $\mathbf{P}(t)$ is expressed as

$$\begin{cases} \mathbf{S}(t) = \mathbf{S}_0(t) + \sum_{k=1}^{m} [\mathbf{S}_{ak}(t)\sin(k\omega_s t) + \mathbf{S}_{bk}(t)\cos(k\omega_s t)] \\ \mathbf{P}(t) = \mathbf{P}_0(t) + \sum_{k=1}^{m} [\mathbf{P}_{ak}(t)\sin(k\omega_s t) + \mathbf{P}_{bk}(t)\cos(k\omega_s t)]. \end{cases} \tag{56}$$

Substituting (56) and (57) into (1), the relationship between the proposed model and the GSSA model is

$$\begin{cases} \mathbf{x}_0(t) = \mathbf{S}_0(t)\mathbf{x}^*(t) + \mathbf{P}_0(t)V_{\text{in}}(t) \\ \mathbf{x}_{ak}(t) = \mathbf{S}_{ak}(t)\mathbf{x}^*(t) + \mathbf{P}_{ak}(t)V_{\text{in}}(t) \\ \mathbf{x}_{bk}(t) = \mathbf{S}_{bk}(t)\mathbf{x}^*(t) + \mathbf{P}_{bk}(t)V_{\text{in}}(t). \end{cases} \tag{57}$$

It can be seen in (57) that the state vectors in the GSSA and MFA models are actually proportional. This is also the reason why they have the same real part of the characteristic root, which is reported in [12].

In the GSSA and MFA models, the first m-order harmonics of the state vector are remained, which can be seen that the first m-order Fourier series of $\mathbf{S}(t)$ and $\mathbf{P}(t)$ is remained in the proposed model. However, the proposed model gives the direct equations of $\mathbf{S}(t)$ and $\mathbf{P}(t)$, which need not to be calculated by Fourier series. Therefore, the GSSA and MFA models are low-order approximations of the proposed model as well. Besides, in the GSSA and MFA models, when the first m-order harmonics are considered, the order of vector and matrices will be $2m+1$ times. However, in the proposed model, the order of vector and matrices is as low as the SSA model. The proposed model is more concise.

TABLE II
PARAMETERS OF VERIFICATION

Parameter	Sign	Value		
		Boost	Buck	Others
Input voltage	V_{in}	24V	40V	24V
Switching frequency	f	20kHz	20kHz	20kHz
Duty cycle	d_1	0.4	0.6	0.6
Inductance	L&L_Z	500μH	500μH	500μH
Capacitance	C&C_Z	20μF	20μF	20μF
ESR of inductor	r_L&r_{LZ}	200mΩ	200mΩ	200mΩ
ESR of capacitor	r_C&r_{LC}	20mΩ	20mΩ	20mΩ
ESR of MOSFET	r_S	40mΩ	40mΩ	40mΩ
ESR of diode	r_D	47.5mΩ	47.5mΩ	47.5mΩ
Load resistance	R_L	20Ω	10Ω	20Ω

ESR: Equivalent Series Resistance

IV. VERIFICATION

In this section, the proposed model and other time-invariant models are established for the basic PWM dc–dc converters. By comparing the results of different models, the advantages of the proposed model are more intuitively demonstrated. The parameters of boost, buck, and buck–boost converters are listed in Table II, their topologies are shown in Fig. 3, and the state matrices and input matrices are listed in Table III, where

$$\begin{aligned} &k_R = R_L/(R_L + r_C), \quad r_1 = r_L + r_S \\ &r_2 = r_L + r_S + k_R r_C, \quad r_3 = r_L + r_D + k_R r_C. \end{aligned} \tag{58}$$

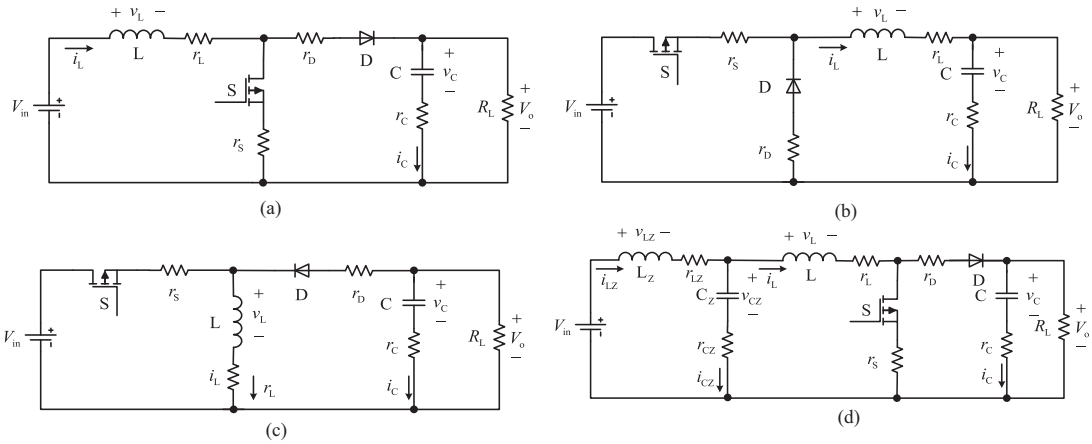

Fig. 3. Topologies of basic PWM dc–dc converters. (a) Boost converter. (b) Buck converter. (c) Buck–boost converter. (d) Boost converter with source impedance.

TABLE III
STATE MATRICES AND INPUT MATRICES OF CONVERTERS

Converter	Boost	Buck	Buck-Boost	Boost with Source Impedance
$\mathbf{x}(t)$	$\begin{bmatrix} i_L & v_C \end{bmatrix}^T$	$\begin{bmatrix} i_L & v_C \end{bmatrix}^T$	$\begin{bmatrix} i_L & v_C \end{bmatrix}^T$	$\begin{bmatrix} i_L & v_C & i_{LZ} & v_{CZ} \end{bmatrix}^T$
$\mathbf{A}_1$	$\begin{bmatrix} -r_1/L & 0 \\ 0 & -k_R/(CR_L) \end{bmatrix}$	$\begin{bmatrix} -r_2/L & -k_R/L \\ k_R/C & -k_R/(CR_L) \end{bmatrix}$	$\begin{bmatrix} -r_1/L & 0 \\ 0 & -k_R/(CR_L) \end{bmatrix}$	$\begin{bmatrix} -(r_1+r_{CZ})/L & 0 & r_{CZ}/L & 1/L \\ 0 & -k_R/(CR_L) & 0 & 0 \\ r_{CZ}/L_Z & 0 & -(r_{LZ}+r_{CZ})/L_Z & -1/L_Z \\ -1/C_Z & 0 & 1/C_Z & 0 \end{bmatrix}$
$\mathbf{A}_2$	$\begin{bmatrix} -r_3/L & -k_R/L \\ k_R/C & -k_R/(CR_L) \end{bmatrix}$	$\begin{bmatrix} -r_3/L & -k_R/L \\ k_R/C & -k_R/(CR_L) \end{bmatrix}$	$\begin{bmatrix} -r_3/L & k_R/L \\ -k_R/C & -k_R/(CR_L) \end{bmatrix}$	$\begin{bmatrix} -(r_3+r_{CZ})/L & -k_R/L & r_{CZ}/L & 1/L \\ k_R/C & -k_R/(CR_L) & 0 & 0 \\ r_{CZ}/L_Z & 0 & -(r_{LZ}+r_{CZ})/L_Z & -1/L_Z \\ -1/C_Z & 0 & 1/C_Z & 0 \end{bmatrix}$
$\mathbf{B}_1$	$\begin{bmatrix} 1/L & 0 \end{bmatrix}^T$	$\begin{bmatrix} 1/L & 0 \end{bmatrix}^T$	$\begin{bmatrix} 1/L & 0 \end{bmatrix}^T$	$\begin{bmatrix} 0 & 0 & 1/L_Z & 0 \end{bmatrix}^T$
$\mathbf{B}_2$	$\begin{bmatrix} 1/L & 0 \end{bmatrix}^T$	$\mathbf{0}$	$\mathbf{0}$	$\begin{bmatrix} 0 & 0 & 1/L_Z & 0 \end{bmatrix}^T$

The state vector of converters can be calculated easily by substituting state matrices and input matrices, as listed in Table III, into the proposed model. The state vectors of other converters, including Cuk, Sepic, and Zeta converters, can be obtained by substituting their state matrices and input matrices into the proposed model similarly. Their parameters are the same as buck–boost converter in this section. Due to the article space limitation, the detail analyses of these converters are not shown. When the converter operates in the closed-loop case or DCM, the duty cycle is decided by state vector and the proposed model is a time-invariant nonlinear model, which is solved by Runge–Kutta method.

A. CCM and Open-Loop Case

When the converter is open loop, the state vector $\mathbf{x}^*(t)$ is calculated by solving

$$\begin{cases} \dot{\mathbf{x}}^*(t) = \mathbf{A}^*\mathbf{x}^*(t) + \mathbf{B}^*V_{\text{in}}(t) \\ \mathbf{x}^*(0) = \mathbf{S}^{-1}(0)[\mathbf{x}(0) - \mathbf{P}(0)V_{\text{in}}(0)]. \end{cases} \tag{59}$$

And when the duty cycle and input voltage are constant, the analytical solution of $\mathbf{x}^*(t)$ is

$$\mathbf{x}^*(t) = e^{\mathbf{A}^*t}\mathbf{x}^*(0) + (e^{\mathbf{A}^*t} - \mathbf{E})\mathbf{A}^{*-1}\mathbf{B}^*V_{\text{in}}(t). \tag{60}$$

Substituting parameters of the boost converter into the proposed model, $\mathbf{A}^*$ and $\mathbf{B}^*$ can be expressed as the polynomial of duty cycle d_1

$$\mathbf{A}^* = \begin{bmatrix} a_{11}(d_1) & a_{12}(d_1) \\ a_{21}(d_1) & a_{22}(d_1) \end{bmatrix} \quad \mathbf{B}^* = \begin{bmatrix} b_1(d_1) \\ b_2(d_1) \end{bmatrix} \tag{61}$$

where

$$a_{11}(d_1) = -83.895d_1^3 + 167.79d_1^2 - 28.935d_1 - 534.96$$
$$a_{12}(d_1) = 0.80098d_1^3 - 2.4491d_1^2 + 1999.7d_1 - 1998.0$$
$$a_{21}(d_1) = -20.025d_1^3 + 61.227d_1^2 - 49991d_1 + 49950$$
$$a_{22}(d_1) = 83.895d_1^3 - 167.79d_1^2 + 83.895d_1 - 2497.5$$
$$b_1(d_1) = -41.577d_1^3 + 83.148d_1^2 - 41.571d_1 + 2000$$
$$b_2(d_1) = -48.128d_1^3 + 143.24d_1^2 - 95.112d_1.$$

When the duty cycle d_1 is 0.4, the value of $\mathbf{A}^*$ and $\mathbf{B}^*$ is

$$\mathbf{A}^* = \begin{bmatrix} -525.06 & -1198.5 \\ 29\,962 & -2485.4 \end{bmatrix} \quad \mathbf{B}^* = \begin{bmatrix} 1994.0 \\ -18.207 \end{bmatrix}. \tag{62}$$

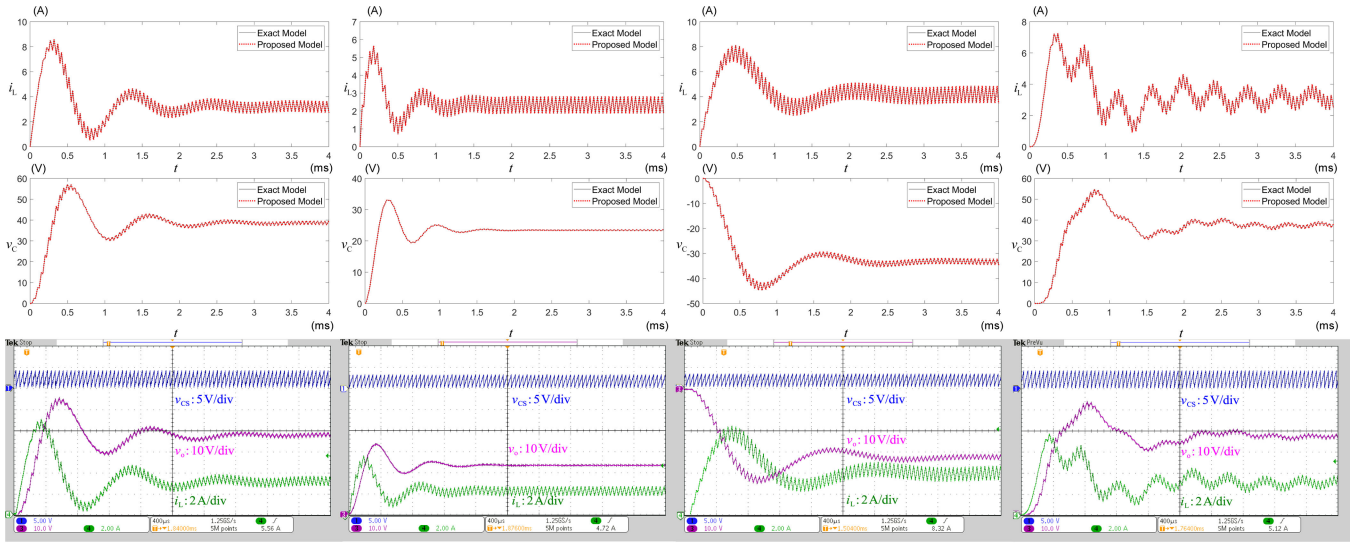

Fig. 4. Dynamic waveforms of converters. (a) Boost. (b) Buck. (c) Buck–boost. (d) Boost with source impedance.

The normalized state vector $\mathbf{x}^*(t)$ is

$$\mathbf{x}^*(t)=\begin{bmatrix} 3.2103-7.8479e^{-1505.2t}\cos(5911.7t+1.2153) \\ 38.523-39.239e^{-1505.2t}\cos(5911.7t-0.19112)\end{bmatrix}. \tag{63}$$

When $\alpha=1$, the original state vector $\mathbf{x}(t)$ is

$$\mathbf{x}(t)=\begin{bmatrix} s_{11}(t_n) & s_{12}(t_n) \\ s_{21}(t_n) & s_{22}(t_n)\end{bmatrix}\mathbf{x}^*(t)+\begin{bmatrix} p_1(t_n) \\ p_2(t_n)\end{bmatrix}V_{\text{in}}(t) \tag{64}$$

where $t_n=t-nT$ and when the converter is in mode 1

$$\begin{aligned}
s_{11}(t_n)&=1.0186e^{1025.2t_n}\cos(5911.7t_n+0.16430)\\
s_{12}(t_n)&=0.20380e^{1025.2t_n}\sin(5911.7t_n)\\
s_{21}(t_n)&=-5.1964e^{-992.26t_n}\sin(5911.7t_n)\\
s_{22}(t_n)&=1.0393e^{-992.26t_n}\cos(5911.7t_n-0.16430)\\
p_1(t_n)&=4.1667-0.33303e^{1025.2t_n}\cos(5911.7t_n-1.1554)\\
&\quad-4.0523e^{-480.00t_n}\\
p_2(t_n)&=-1.6991e^{-992.26t_n}\cos(5911.7t_n+0.25112)\\
&\quad+1.6458e^{-2497.5t_n}.
\end{aligned}$$

When the converter is in mode 2

$$\begin{aligned}
s_{11}(t_n)&=1.0256e^{-10.992t_n}\cos(4030.0t_n-0.33150)\\
&\quad+0.035652e^{-10.992t_n}\cos(15\,853t_n+1.1081)\\
s_{12}(t_n)&=0.20511e^{-10.992t_n}\cos(4030.0t_n+1.4036)\\
&\quad+0.0071305e^{-10.992t_n}\cos(15\,853t_n-0.62705)\\
s_{21}(t_n)&=-5.1278e^{-10.992t_n}\cos(4030.0t_n+1.3377)\\
&\quad+0.17826e^{-10.992t_n}\cos(15\,853t_n-0.36436)\\
s_{22}(t_n)&=1.0256e^{-10.992t_n}\cos(4030.0t_n-0.068820)\\
&\quad-0.035652e^{-10.992t_n}\cos(15\,853t_n+1.0421)\\
p_1(t_n)&=0.049389-0.011657e^{-10.992t_n}\\
&\quad\times\cos(15\,853t_n-0.21162)\\
&\quad-0.33533e^{-10.992t_n}\cos(4030.0t_n+0.98816)\\
&\quad+0.15276e^{-1516.2t_n}\cos(9941.7t_n+0.5971)\\
p_2(t_n)&=0.98778+0.058286e^{-10.992t_n}\\
&\quad\times\cos(15\,853t_n+1.4576)\\
&\quad-1.6766e^{-10.992t_n}\cos(4030.0t_n-0.48425)\\
&\quad+0.76381e^{-1516.2t_n}\cos(9941.7t_n-0.87532).
\end{aligned}$$

The waveforms of (64) are shown in Fig. 4(a). Similarly, the waveforms of buck and buck–boost converters are obtained and shown in Fig. 4(b) and (c). As shown in Fig. 4, the proposed model can reflect the dynamic characteristics of the converter exactly.

When $\alpha=1$, the results of the SSA model, the GSSA model, the second-order KBM model, and the proposed model are compared with the results of the time-variant exact model in Fig. 5. In the SSA model, the waveforms contain no ripple. In the GSSA model, the ripples are expressed by trigonometric functions. However, the exact waveforms are closer to triangular wave. The GSSA model is not very consistent with the exact model. In the KBM model, the ripple is calculated using the results of the SSA model. For the inductor current, as the results of the SSA model are accurate, the results of the KBM model are accurate as well. For capacitor voltages, as the SSA model cannot reflect the average behaviors of converters accurately, the KBM model has a large error. In the proposed model, all waveforms agree well with the results of the exact model.

In order to show the accuracy of the proposed model, the mean relative errors (MREs) of state variables are calculated and listed

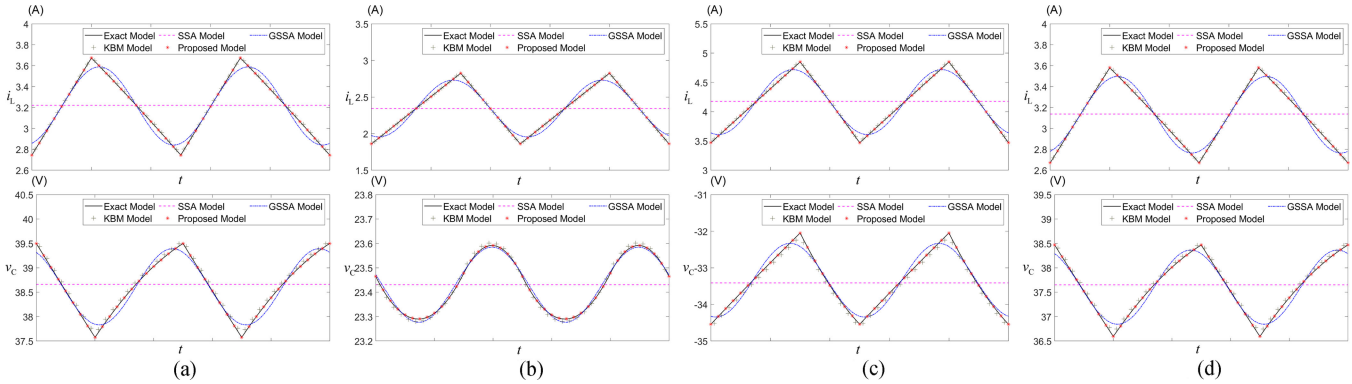

Fig. 5. Steady waveforms of converters. (a) Boost. (b) Buck. (c) Buck–boost. (d) Boost with source impedance.

TABLE IV
MREs OF THE PROPOSED MODEL AND OTHER MODELS

Converter	SSA	GSSA	KBM	Proposed
Boost	4.3003%	0.7191%	0.1818%	0.0006%
Buck	5.4818%	0.8951%	0.0960%	0.0040%
Buck-Boost	5.1656%	0.8772%	0.1402%	0.0004%
Boost with Impedance	2.3185%	0.3698%	0.1540%	0.0047%
Cuk	9.5028%	1.5817%	0.2510%	0.0145%
Sepic	10.384%	1.7724%	0.3041%	0.0062%
Zeta	9.7003%	1.6186%	0.2599%	0.0160%

TABLE V
AVERAGE VALUES OF THE OUTPUT CAPACITOR VOLTAGE

Converter	Exact	SSA	GSSA	KBM	Proposed
Boost	38.610V	38.661V	38.612V	38.661V	38.610V
Buck	23.431V	23.431V	23.431V	23.431V	23.431V
Buck-Boost	-33.336V	-33.413V	-33.339V	-33.413V	-33.336V
Boost with Impedance	37.602V	37.651V	37.604V	37.651V	37.602V
Cuk	-34.401V	-34.370V	-34.399V	-34.370V	-34.400V
Sepic	34.206V	34.321V	34.210V	34.321V	34.205V
Zeta	34.401V	34.370V	34.400V	34.370V	34.400V

in Table IV. The average value of output capacitor voltage v_C is calculated and listed in Table V. The MRE of the SSA model is large as all ripples are ignored, the MREs of the GSSA model and the KBM model are lower than the SSA model, and the MRE of the proposed model is minimum, which is lower than 0.1%. The proposed model is more accurate than the other models. For the average value of the output capacitor voltage, the errors of the SSA model and the KBM model are much larger than those of the GSSA model and the proposed model. The SSA model and the KBM model contain low-frequency errors, which are negligible in the GSSA model and the proposed model.

In order to further verify the generality of the proposed model, the boost converter with different carriers ($\alpha = 0$ and 0.5) and

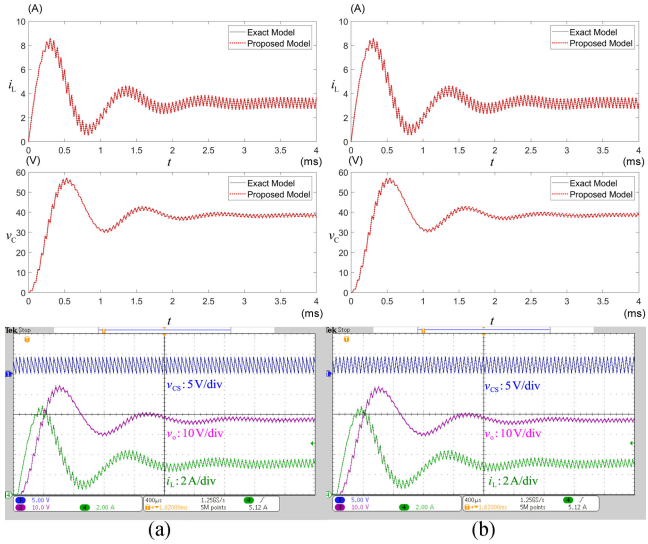

Fig. 6. Dynamic waveforms of the boost converters with different carriers. (a) $\alpha = 0$. (b) $\alpha = 0.5$.

the buck converter with different duty cycles ($d_1 = 0.2$ and 0.8) are modeled by the proposed method. As shown in Figs. 6 and 7, the proposed model can accurately reflect the dynamic characteristics of the converter under these circumstances. When the converter operates in steady state, the MRE of state variables under these circumstances is 0.0007%, 0.0006%, 0.0084%, and 0.0018%, respectively. The proposed model can reflect the steady characteristics of the converters as well.

B. CCM and Closed-Loop Case

The boost, buck, and buck–boost converters with the proportional integral (PI) controller are modeled by the proposed method, whose results are compared with the results of the exact model. The reference voltages of the boost, buck, and buck–boost converters are 40, 24, and −36 V, respectively. The transfer function of the PI controller is

$$G_{\mathrm{PI}}(s) = K_{\mathrm{P}} + \frac{1}{s}K_{\mathrm{I}} = \frac{s + 5000}{1000s} \tag{65}$$

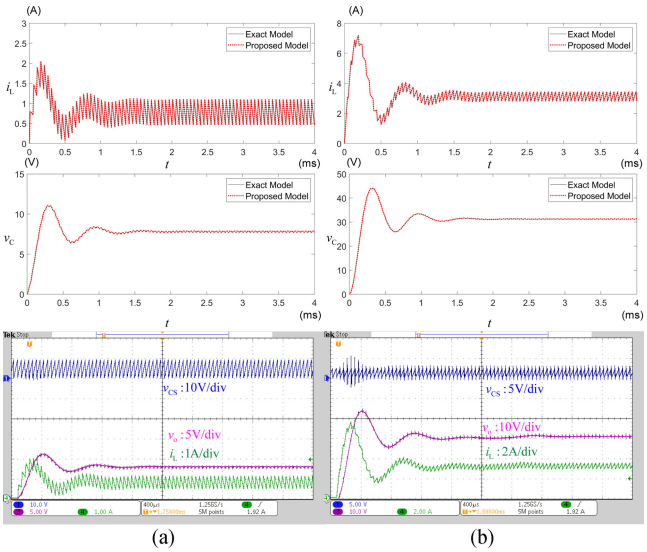

Fig. 7. Dynamic waveforms of the buck converters with different duty cycles. (a) $d = 0.2$. (b) $d = 0.8$.

where K_P and K_I are the proportionality coefficient and integral coefficient of the PI controller, respectively.

The transfer function of the PI controller in (65) is equal to the following state-space equation:

$$\begin{cases} \dot{x}_C(t) = K_I(V_{ref} - v_o) \\ d_C(t) = x_C(t) + K_P(V_{ref} - v_o) \end{cases} \tag{66}$$

where $x_C(t)$ is the state variable of the PI controller. Then, the converter with PI controller can be solved with the proposed method.

Assuming that $\alpha = 1$, $\mathbf{x}(0) = \mathbf{0}$, and the initial conditions of integrator $x_C(0)$ in boost, buck and buck–boost converter are 0.4, 0.6, and 0.6, respectively, the proposed model is calculated and the waveforms of $\mathbf{x}(t)$ are obtained. The dynamic waveforms of converters with PI controller are shown in Fig. 8. The results of the proposed model match the results of the exact model and experiment accurately. In addition, when converters are in steady state, the MREs of the state vector in boost, buck, and buck–boost converters are 0.0813%, 0.0858%, and 0.0033%, respectively. Therefore, the proposed model can reflect both the dynamic and steady-state behavior of converters during the closed-loop operation.

In order to further verify the generality of the proposed model, when $\alpha = 1$, the buck–boost converter with load resistance and reference output voltage changes is modeled by the proposed method, whose results are shown in Fig. 9. Compared with a zero-state startup, the only difference is that the $\mathbf{x}(0)$ is decided by the state vectors before parameters change. Before parameter changing, the converter is in the steady state. In case 1, the reference output voltage V_{ref} is added from -36 to -24 V. In case 2, the V_{ref} is reduced from -24 to -36 V. In case 3, the load resistance R_L is added from 20 to 30 Ω. In case 4, the R_L is reduced from 30 to 20 Ω. As shown in Fig. 9, the proposed model can reflect the dynamic behavior of converter under these circumstances.

C. DCM Case

When the converter operates at DCM, substituting the matrices of boost converter into (29) and remaining the linear term of switching period T, it is obtained that

$$d_2 \approx -\frac{\mathbf{K}[(\mathbf{E} + 0.5\mathbf{A}_1 d_1 T)\mathbf{x}^* + 0.5 d_1 T \mathbf{B}_1 V_{in})]}{\mathbf{K}(\mathbf{A}_2\mathbf{x}^* + \mathbf{B}_2 V_{in})T} \tag{67}$$

where

$$\mathbf{K} = \begin{bmatrix} 1 & 0 \end{bmatrix}. \tag{68}$$

The state matrix and the input matrix of a boost converter in mode 3 are

$$\mathbf{A}_3 = \begin{bmatrix} -r_3/L & -k_R/L \\ k_R/C & -k_R/(CR_L) \end{bmatrix} \tag{69}$$

$$\mathbf{B}_3 = \begin{bmatrix} 0 & 0 \end{bmatrix}^T. \tag{70}$$

The waveform of the boost converter that operates in DCM is shown in Fig. 10. In case 1, the boost converter operates in the open-loop state and the load resistance is increased from 200 to 300 Ω. In case 2, the boost converter operates in the open-loop state and the load resistance is decreased from 300 to 200 Ω. In case 3, the boost converter operates in the closed-loop state and the load resistance is increased from 200 to 300 Ω. In case 4, the boost converter operates in the closed-loop state and the load resistance is decreased from 300 to 200 Ω. Other parameters are the same as the boost converter with CCM, as listed in Table II. The proposed model can reflect the behavior of the converter operating in DCM.

D. Frequency-Domain Analysis

The proposed model can be used to analyze the influence of the switching period on the stability of the converter. The boost converter with PI controller is discussed here. In this section, the unmentioned parameters of the converter are listed in Table II.

In case 1, α is 1, K_P is 0.012, and K_I is 5. When the switching frequency is 20 kHz, the open-loop transfer function obtained by the proposed model is

$$G_{op}(s) = \frac{2.21 \times 10^{-2} s^3 - 2365 s^2 + 2.59 \times 10^7 s + 1.14 \times 10^{10}}{s^3 + 3009 s^2 + 3.458 \times 10^7 s}. \tag{71}$$

When the switching frequency is 5 kHz, the open-loop transfer function obtained by the proposed model is

$$G_{op}(s) = \frac{8.89 \times 10^{-2} s^3 - 3227 s^2 + 2.61 \times 10^7 s + 1.11 \times 10^{10}}{s^3 + 3009 s^2 + 3.462 \times 10^7 s}. \tag{72}$$

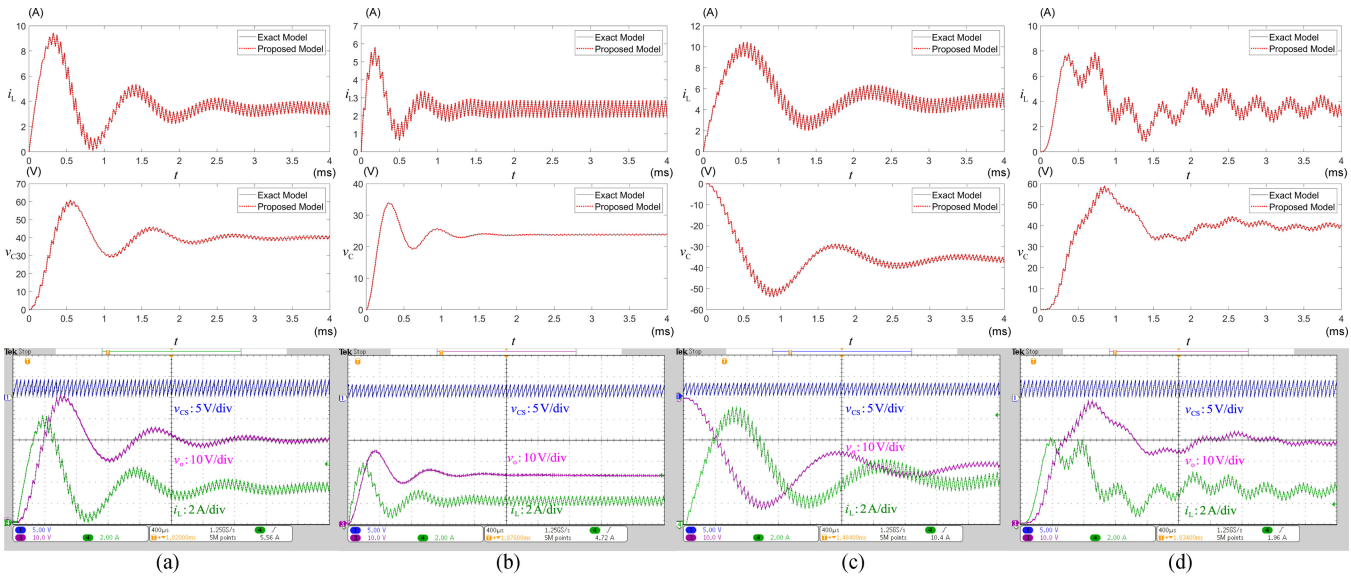

Fig. 8. Dynamic waveforms of the converters with PI controller. (a) Boost. (b) Buck. (c) Buck–boost. (d) Boost with source impedance.

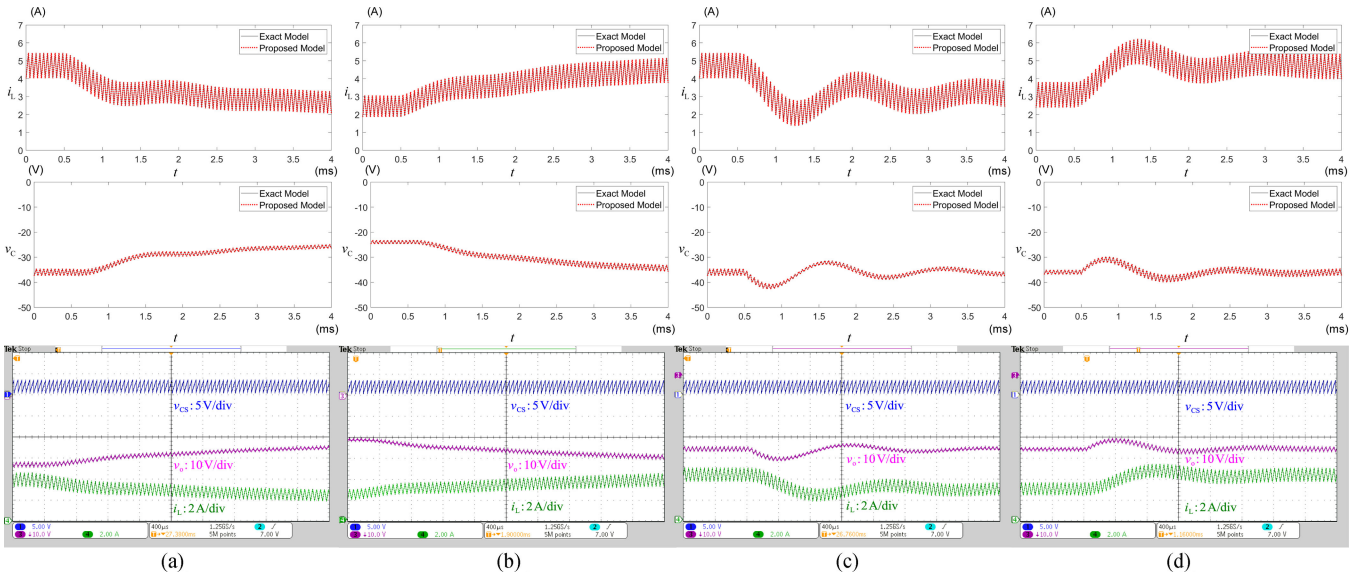

Fig. 9. Dynamic waveforms of the buck–boost converter with load resistance and reference output voltage changes. (a) Case 1. (b) Case 2. (c) Case 3. (d) Case 4.

And the open-loop transfer function obtained by the SSA model is always

$$G_{\rm op}(s) = \frac{-8.31\times10^{-4}s^3 - 2068s^2 + 2.59\times10^7 s + 1.11\times10^{10}}{s^3 + 3009s^2 + 3.457\times10^7 s}. \tag{73}$$

Their bode diagrams are shown in Fig. 11(a) and (b). The magnitude margin obtained by (71)–(73) is 1.46, −1.15, and 2.61 dB, respectively. As shown in Fig. 11(c), when the switching frequency is 20 kHz, the converter is stable. The two model can both reflect the stability of the converter. As shown in Fig. 11(d), when the switching frequency is 5 kHz, the converter is unstable, only the proposed model can reflect the stability of the converter.

In case 2, α is 0, $K_{\rm P}$ is 0.02, and $K_{\rm I}$ is 10. When the switching frequency is 20 kHz, the open-loop transfer function obtained by the proposed model is

$$G_{\rm op}(s) = \frac{-3.80\times10^{-2}s^3 - 3034s^2 + 4.18\times10^7 s + 2.09\times10^{10}}{s^3 + 3009s^2 + 3.31\times10^7 s}. \tag{74}$$

When the switching frequency is 5 kHz, the open-loop transfer function obtained by the proposed model is

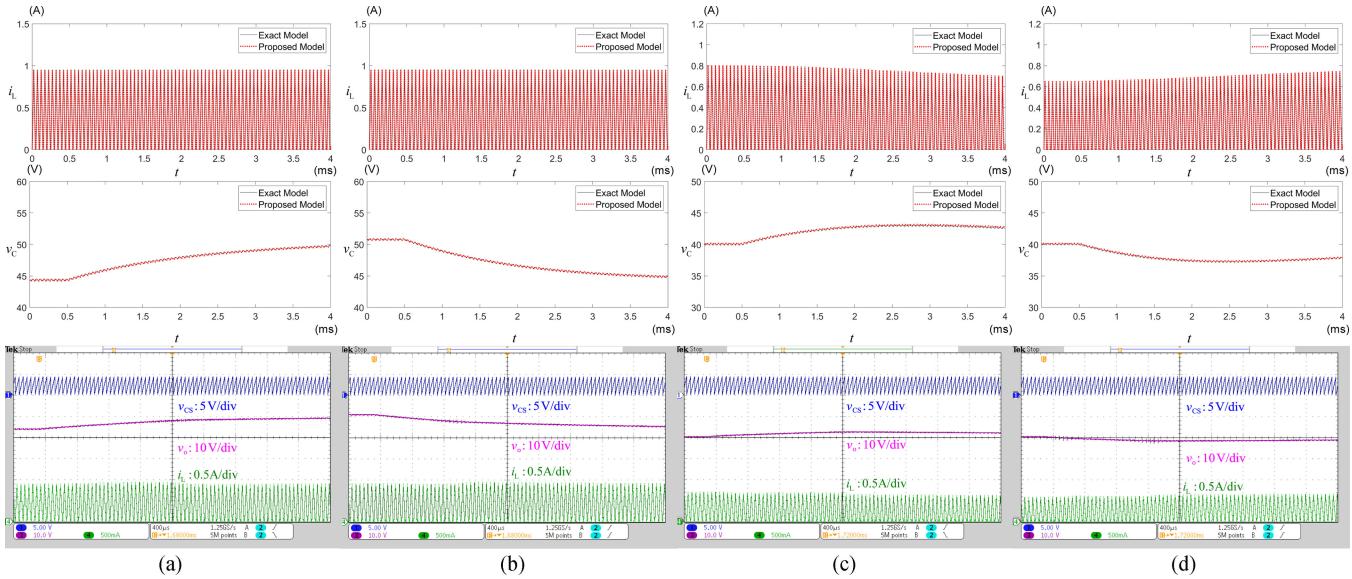

Fig. 10. Dynamic waveforms of boost converter operate in DCM. (a) Case 1. (b) Case 2. (c) Case 3. (d) Case 4.

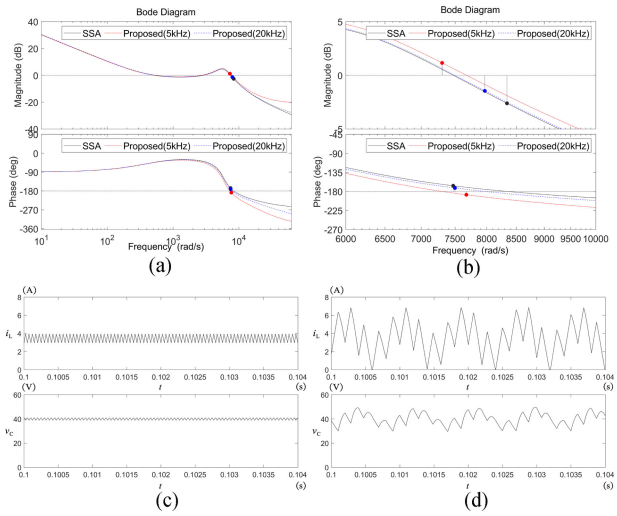

Fig. 11. Frequency-domain analysis of case 1. (a) Bode diagram. (b) Partial enlarged drawing. (c) Simulation results of 20 kHz. (d) Simulation results of 5 kHz.

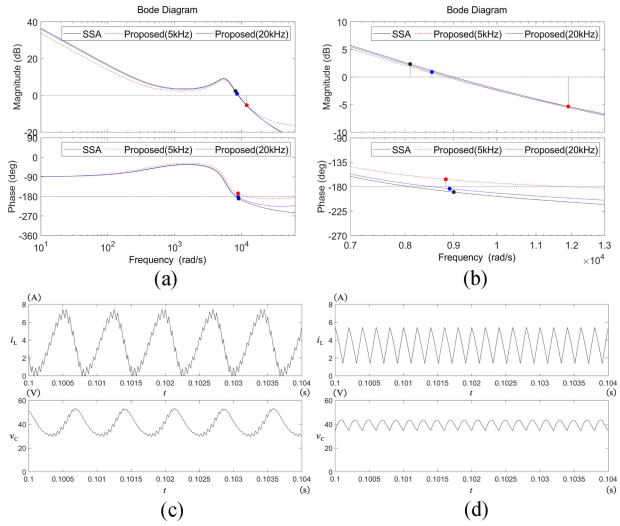

Fig. 12. Frequency-domain analysis of case 2. (a) Bode diagram. (b) Partial enlarged drawing. (c) Simulation results of 20 kHz. (d) Simulation results of 5 kHz.

$$G_{\rm op}(s) = \frac{-1.38\times10^{-1}s^3 - 1485s^2 + 3.93\times10^7 s + 1.61\times10^{10}}{s^3 + 3009s^2 + 3.31\times10^7 s}. \tag{75}$$

And the open-loop transfer function obtained by the SSA model is always

$$G_{\rm op}(s) = \frac{-1.50\times10^{-2}s^3 - 3608s^2 + 4.26\times10^7 s + 2.22\times10^{10}}{s^3 + 3009s^2 + 3.30\times10^7 s}. \tag{76}$$

Their bode diagrams are shown in Fig. 12(a) and (b). The magnitude margin obtained by (74)–(76) is -0.85, 5.51, and -2.36 dB, respectively. As shown in Fig. 12(c), when the switching frequency is 20 kHz, the converter is unstable. The two model can both reflect the stability of the converter. As shown in Fig. 12(d), when the switching frequency is 5 kHz, the converter is stable, and only the proposed model can reflect the stability of converter.

V. Conclusion

In this article, a time-invariant polynomial model of fixed-frequency PWM dc–dc converter is proposed. Through normalized coordinate transformation, the time-varying model of the converter is transferred into a time-invariant model, whose

state matrix and input matrix are obtained by the addition and multiplication of matrices simply and expressed by the polynomial of duty cycle concisely. The proposed model has the following advantages. Compared with the SSA model, the ripple of the state vector and the switching period are considered, thereby improving the accuracy. Contrary to other time-invariant models, the state matrix and input matrix instead of the state vector are expanded into series. Therefore, neither the number of state vectors nor the order of the matrices increases, and the proposed model has a simple structure similar to the SSA model. In addition, as a time-invariant polynomial model, the calculation and analysis of the proposed model are much simpler than the time-variant exact model.

In order to demonstrate the advantages of the proposed model more intuitively, several basic converters are modeled by the proposed method, whose results are compared with other models' results. Compared with the SSA model, the GSSA model, and the KBM model, the waveforms of state variables in the proposed model are more accurate. Compared with the exact model, the maximum error of the proposed model is less than 0.1%. Besides, the proposed model can be used to analyze the influence of the switching period on the stability of the converter. The simulation and experimental results ensure the validity of the above-mentioned analyses and advantages. Therefore, the proposed model is suitable for the model of fixed-frequency PWM dc–dc converter when both simple structure and high accuracy are needed.

APPENDIX

A. Formula of State Matrix

In order to obtain the formula of $\mathbf{A}_p^*$, first, (15) is substituted into the $e^{\mathbf{A}^*T}$ in (12)

$$\begin{aligned} e^{\mathbf{A}^*T} &= \mathbf{E} + \sum_{p=0}^{\infty} \mathbf{A}_p^* T^{p+1} + \sum_{q=2}^{\infty} \frac{(\sum_{p=0}^{\infty} \mathbf{A}_p^* T^{p+1})^q}{q!} \\ &= \mathbf{E} + \sum_{p=0}^{\infty} \mathbf{A}_p^* T^{p+1} + \sum_{q=2}^{\infty} \frac{\sum_{n_0=0}^{\infty} \cdots \sum_{n_{q-1}=0}^{\infty} \prod_{j=0}^{q-1} \mathbf{A}_{n_j}^*}{q!} \\ &\quad \times T^{q+\sum_{j=0}^{q-1} n_j} \\ &= \mathbf{E} + \sum_{p=0}^{\infty} \mathbf{A}_p^* T^{p+1} + \sum_{p=1}^{\infty} \sum_{r=0}^{p-1} \frac{\sum \mathbf{Y}}{(r+2)!} T^{p+1} \end{aligned} \tag{A1}$$

where the matrix $\mathbf{Y}$ satisfies

$$\mathbf{Y} \in \mathbf{Y}^*(p,r) = \{\, \mathbf{Y} |\ \mathbf{Y} = \prod_{j=0}^{r+1} \mathbf{A}_{n_j}^*,\ \textstyle\sum_{j=0}^{r+1} n_j = p-1-r \,\}. \tag{A2}$$

Then, substituting (14) into (12), for the converter that operates in DCM, $e^{\mathbf{A}^*T}$ can be expressed as

$$\begin{aligned} e^{\mathbf{A}^*T} &= e^{0.5\mathbf{A}_1 d_1 T} e^{\mathbf{A}_3 d_3 T} e^{\mathbf{A}_2 d_2 T} e^{0.5\mathbf{A}_1 d_1 T} \\ &= \sum_{m=0}^{\infty} \frac{\mathbf{A}_1^m d_1^m T^m}{2^m m!} \sum_{m=0}^{\infty} \frac{\mathbf{A}_3^m d_3^m T^m}{m!} \sum_{m=0}^{\infty} \frac{\mathbf{A}_2^m d_2^m T^m}{m!} \\ &\quad \times \sum_{m=0}^{\infty} \frac{\mathbf{A}_1^m d_1^m T^m}{2^m m!} \\ &= \sum_{k=0}^{\infty} \left(\sum_{i+j+m+n=k} \frac{d_1^{m+n} d_2^i d_3^j \mathbf{A}_1^m \mathbf{A}_2^i \mathbf{A}_3^j \mathbf{A}_1^n}{2^{m+n} m! n! i! j!} \right) T^k. \end{aligned} \tag{A3}$$

Let k be equal to $p+1$ and (A3) can be simplified into

$$\begin{aligned} e^{\mathbf{A}^*T} &= \mathbf{E} + (d_1\mathbf{A}_1 + d_2\mathbf{A}_2 + d_3\mathbf{A}_3)T \\ &\quad + \sum_{p=1}^{\infty} \left(\sum_{i+j+m+n=p+1} \frac{d_1^{m+n} d_2^i d_3^j \mathbf{A}_1^m \mathbf{A}_2^i \mathbf{A}_3^j \mathbf{A}_1^n}{2^{m+n} m! n! i! j!} \right) T^{p+1}. \end{aligned} \tag{A4}$$

The formula of $\mathbf{A}_p^*$ is obtained by comparing the coefficient of T^{p+1} in (A1) and (A4). When the converter operates in CCM, the formula of $\mathbf{A}_p^*$ can be obtained by substituting $d_3 = 0$ into the above equations.

B. Formula of Input Matrix

When the converter operates in DCM, first, (14) is substituted into (13), and $\mathbf{B}^*$ can be expressed as

$$\begin{aligned} \mathbf{B}^* &= \mathbf{A}^*(e^{\mathbf{A}^*T} - \mathbf{E})^{-1}(e^{0.5\mathbf{A}_1 d_1 T} e^{\mathbf{A}_3 d_3 T} e^{\mathbf{A}_2 d_2 T} + \mathbf{E}) \\ &\quad \times (e^{0.5\mathbf{A}_1 d_1 T} - \mathbf{E})\mathbf{A}_1^{-1}\mathbf{B}_1 \\ &\quad + \mathbf{A}^*(e^{\mathbf{A}^*T} - \mathbf{E})^{-1} e^{0.5\mathbf{A}_1 d_1 T} e^{\mathbf{A}_3 d_3 T}(e^{\mathbf{A}_2 d_2 T} - \mathbf{E}) \\ &\quad \times \mathbf{A}_2^{-1}\mathbf{B}_2 \\ &\quad + \mathbf{A}^*(e^{\mathbf{A}^*T} - \mathbf{E})^{-1} e^{0.5\mathbf{A}_1 d_1 T}(e^{\mathbf{A}_3 d_3 T} - \mathbf{E})\mathbf{A}_3^{-1}\mathbf{B}_3. \end{aligned} \tag{B1}$$

Second, (20) is substituted into (15), and $\mathbf{A}^*$ can be expressed as

$$\begin{aligned} \mathbf{A}^* &= \sum_{p=0}^{\infty} \mathbf{A}_p^* T^p = \sum_{p=0}^{\infty} (\mathbf{F}_{p1}^* \mathbf{A}_1 + \mathbf{F}_{p2}^* \mathbf{A}_2 + \mathbf{F}_{p3}^* \mathbf{A}_3) T^p \\ &= \sum_{p=0}^{\infty} \mathbf{F}_{p1}^* T^p \mathbf{A}_1 + \sum_{p=0}^{\infty} \mathbf{F}_{p2}^* T^p \mathbf{A}_2 + \sum_{p=0}^{\infty} \mathbf{F}_{p3}^* T^p \mathbf{A}_3. \end{aligned} \tag{B2}$$

Third, through the matrix identity transformation, $\mathbf{A}^*$ can also be expressed as

$$\begin{aligned} \mathbf{A}^* &= \mathbf{A}^*(e^{\mathbf{A}^*T} - \mathbf{E})^{-1}(e^{\mathbf{A}^*T} - \mathbf{E}) \\ &= \mathbf{A}^*(e^{\mathbf{A}^*T} - \mathbf{E})^{-1}(e^{0.5\mathbf{A}_1 d_1 T} e^{\mathbf{A}_3 d_3 T} e^{\mathbf{A}_2 d_2 T} e^{0.5\mathbf{A}_1 d_1 T} - \mathbf{E}) \\ &= \mathbf{A}^*(e^{\mathbf{A}^*T} - \mathbf{E})^{-1}(e^{0.5\mathbf{A}_1 d_1 T} e^{\mathbf{A}_3 d_3 T} e^{\mathbf{A}_2 d_3 T} + \mathbf{E})(e^{0.5\mathbf{A}_1 d_1 T} \\ &\quad - \mathbf{E})\mathbf{A}_1^{-1}\mathbf{A}_1 \\ &\quad + \mathbf{A}^*(e^{\mathbf{A}^*T} - \mathbf{E})^{-1} e^{0.5\mathbf{A}_1 d_1 T} e^{\mathbf{A}_3 d_3 T}(e^{\mathbf{A}_2 d_2 T} - \mathbf{E})\mathbf{A}_2^{-1}\mathbf{A}_2 \\ &\quad + \mathbf{A}^*(e^{\mathbf{A}^*T} - \mathbf{E})^{-1} e^{0.5\mathbf{A}_1 d_1 T}(e^{\mathbf{A}_3 d_3 T} - \mathbf{E})\mathbf{A}_3^{-1}\mathbf{A}_3. \end{aligned} \tag{B3}$$

Fourth, compare (B2) with (B3), it is obtained that

$$\begin{cases} \sum_{p=0}^{\infty} \mathbf{F}_{p1}^{*} T^{p} = \mathbf{A}^{*}(e^{\mathbf{A}^{*}T} - \mathbf{E})^{-1}(e^{0.5\mathbf{A}_1 d_1 T} e^{\mathbf{A}_3 d_3 T} e^{\mathbf{A}_2 d_3 T} + \mathbf{E}) \\ (e^{0.5\mathbf{A}_1 d_1 T} - \mathbf{E})\mathbf{A}_1^{-1} \\ \sum_{p=0}^{\infty} \mathbf{F}_{p2}^{*} T^{p} = \mathbf{A}^{*}(e^{\mathbf{A}^{*}T} - \mathbf{E})^{-1} e^{0.5\mathbf{A}_1 d_1 T} e^{\mathbf{A}_3 d_3 T} \\ (e^{\mathbf{A}_2 d_2 T} - \mathbf{E})\mathbf{A}_2^{-1} \\ \sum_{p=0}^{\infty} \mathbf{F}_{p2}^{*} T^{p} = \mathbf{A}^{*}(e^{\mathbf{A}^{*}T} - \mathbf{E})^{-1} e^{0.5\mathbf{A}_1 d_1 T}(e^{\mathbf{A}_3 d_3 T} - \mathbf{E})\mathbf{A}_3^{-1}. \end{cases} \tag{B4}$$

Finally, substituting (16) and (B4) into (B1), it is proved that the formula of $\mathbf{B}_p^{*}$ is (21).

$$\begin{aligned} \mathbf{B}^{*} &= \sum_{p=0}^{\infty} \mathbf{F}_{p1}^{*} T^{p} \mathbf{B}_1 + \sum_{p=0}^{\infty} \mathbf{F}_{p2}^{*} T^{p} \mathbf{B}_2 + \sum_{p=0}^{\infty} \mathbf{F}_{p3}^{*} T^{p} \mathbf{B}_3 \\ &= \sum_{p=0}^{\infty} \mathbf{B}_p^{*} T^{p}. \end{aligned} \tag{B5}$$

When the converter operates in CCM, the proof can be obtained by substituting $d_3 = 0$ into (B1)–(B5).

C. Formula of Transfer Function

When the converter is in steady state, the augmented state vector and the augmented input vector satisfy

$$\dot{\mathbf{x}}_{\mathrm{au}}^{*} = \mathbf{A}_{\mathrm{au}}{}^{*}\mathbf{x}_{\mathrm{au}}{}^{*} + \mathbf{B}_{\mathrm{au}}{}^{*}\mathbf{u} = 0. \tag{C1}$$

Substituting (C1) into (1), it is obtained that

$$\begin{aligned} &\mathbf{x}_{\mathrm{au}}(nT + (\alpha - 0.5)d_1 T) \\ &\quad = \mathbf{S}(nT + (\alpha - 0.5)d_1 T)\mathbf{x}_{\mathrm{au}}^{*} + \mathbf{P}_{\mathrm{au}}(nT + (\alpha - 0.5)d_1 T)\mathbf{u} \\ &\quad = e^{-\mathbf{A}_{\mathrm{au}}^{*}(\alpha - 0.5)d_1 T}\mathbf{x}_{\mathrm{au}}^{*} + (e^{-\mathbf{A}_{\mathrm{au}}^{*}(\alpha - 0.5)d_1 T} - \mathbf{E})\mathbf{A}_{\mathrm{au}}^{*}{}^{-1}\mathbf{B}_{\mathrm{au}}^{*}\mathbf{u} \\ &\quad = \mathbf{x}_{\mathrm{au}}^{*}. \end{aligned} \tag{C2}$$

Substituting (C1) into (33), it is obtained that

$$\begin{aligned} &d_{\mathrm{C}}(nT + \alpha d_1 T) \\ &\quad = \mathbf{C}_{\mathrm{au}1}[e^{0.5\mathbf{A}_1 d_1 T}\mathbf{x}_{\mathrm{au}}(nT + (\alpha - 0.5)d_1 T) \\ &\qquad + (e^{0.5\mathbf{A}_1 d_1 T} - \mathbf{E})\mathbf{A}_1^{-1}\mathbf{B}_1\mathbf{u}] \end{aligned} \tag{C3}$$

$$\begin{aligned} &d_{\mathrm{C}}(nT + T - (1 - \alpha)d_1 T) = d_{\mathrm{C}}(nT - (1 - \alpha)d_1 T) \\ &\quad = \mathbf{C}_{\mathrm{au}2}[e^{-0.5\mathbf{A}_1 d_1 T}\mathbf{x}_{\mathrm{au}}(nT + (\alpha - 0.5)d_1 T) \\ &\qquad + (e^{-0.5\mathbf{A}_1 d_1 T} - \mathbf{E})\mathbf{A}_1^{-1}\mathbf{B}_1\mathbf{u}]. \end{aligned} \tag{C4}$$

Using small-signal analysis and ignoring $\hat{\mathbf{u}}$, (C3) and (C4) can be expressed as

$$\begin{aligned} \hat{d}_{\mathrm{C}1} &= \hat{d}_{\mathrm{C}}(nT + \alpha d_1 T) \\ &= \mathbf{C}_{\mathrm{au}1} e^{0.5\mathbf{A}_1 \bar{d}_1 T}[\hat{\mathbf{x}}_{\mathrm{au}}(nT + (\alpha - 0.5)d_1 T) \\ &\qquad + 0.5T(\mathbf{A}_1\bar{\mathbf{x}}_{\mathrm{au}}^{*} + \mathbf{B}_1\bar{\mathbf{u}})\hat{d}_1] \end{aligned} \tag{C5}$$

$$\begin{aligned} \hat{d}_{\mathrm{C}2} &= \hat{d}_{\mathrm{C}}(nT - (1 - \alpha)d_1 T) = \hat{d}_{\mathrm{C}}(nT + (\alpha - 1)d_1 T) \\ &= \mathbf{C}_{\mathrm{au}2} e^{-0.5\mathbf{A}_1 \bar{d}_1 T}[\hat{\mathbf{x}}_{\mathrm{au}}(nT + (\alpha - 0.5)d_1 T) \\ &\qquad - 0.5T(\mathbf{A}_1\bar{\mathbf{x}}_{\mathrm{au}}^{*} + \mathbf{B}_1\bar{\mathbf{u}})\hat{d}_1]. \end{aligned} \tag{C6}$$

Using the time delay nature of the Laplace transform, the frequency-domain equations of (C5) and (C6) can be expressed as

$$\begin{cases} \hat{d}_{\mathrm{C}1}(s) = \mathbf{C}_{\mathrm{au}1} e^{0.5\mathbf{A}_1 \bar{d}_1 T}[e^{-0.5\bar{d}_1 T s}\hat{\mathbf{x}}_{\mathrm{au}}^{*}(s) \\ \qquad\qquad + 0.5T(\mathbf{A}_1\bar{\mathbf{x}}_{\mathrm{au}}^{*} + \mathbf{B}_1\bar{\mathbf{u}})\hat{d}_1(s)] \\ \hat{d}_{\mathrm{C}2}(s) = \mathbf{C}_{\mathrm{au}2} e^{-0.5\mathbf{A}_1 \bar{d}_1 T}[e^{0.5\bar{d}_1 T s}\hat{\mathbf{x}}_{\mathrm{au}}^{*}(s) \\ \qquad\qquad - 0.5T(\mathbf{A}_1\bar{\mathbf{x}}_{\mathrm{au}}^{*} + \mathbf{B}_1\bar{\mathbf{u}})\hat{d}_1(s)]. \end{cases} \tag{C7}$$

Using small-signal analysis, (35) can be expressed as

$$\hat{d}_1(s) = \alpha\hat{d}_{\mathrm{C}1}(s) + (1 - \alpha)\hat{d}_{\mathrm{C}2}(s). \tag{C8}$$

Substituting (C7) into (C8), (42) is proven.

REFERENCES

[1] Y. Song and B. Wang, "Survey on reliability of power electronic systems," *IEEE Trans. Power Electron.*, vol. 28, no. 1, pp. 591–604, Jan. 2013.

[2] R. D. Middlebrook and S. Cuk, "A general unified approach to modelling switching-converter power stages," *Int. J. Electron.*, vol. 42, no. 6, pp. 521–550, 1977.

[3] B. Lehman and R. M. Bass, "Extensions of averaging theory for power electronic systems," *IEEE Trans. Power Electron.*, vol. 11, no. 4, pp. 542–553, Jul. 1996.

[4] D. J. Shortt and F. C. Lee, "Extensions of the discrete-average models for converter power stages," *IEEE Trans. Aerosp. Electron. Syst.*, vol. AES-20, no. 3, pp. 279–289, May 1984.

[5] M. Veerachary, "General rules for signal flow graph modeling and analysis of DC-DC converters," *IEEE Trans. Aerosp. Electron. Syst.*, vol. 40, no. 1, pp. 259–271, Jan. 2004.

[6] S. R. Sanders, J. M. Noworolski, X. Z. Liu, and G. C. Verghese, "Generalized averaging method for power conversion circuits," *IEEE Trans. Power Electron.*, vol. 6, no. 2, pp. 251–259, Apr. 1991.

[7] J. Xu and C. Q. Lee, "Generalized state-space averaging approach for a class of periodically switched network," *IEEE Trans. Circuits Syst. I, Fundam. Theory Appl.*, vol. 44, no. 11, pp. 1078–1081, Nov. 1997.

[8] A. Emadi, "Modeling and analysis of multiconverter dc power electronic systems using the generalized state-space averaging method," *IEEE Trans. Ind. Electron.*, vol. 51, no. 3, pp. 661–668, Jun. 2004.

[9] H. Qin and J. W. Kimball, "Generalized averaging modeling of dual active bridge dc-dc converter," *IEEE Trans. Power Electron.*, vol. 27, no. 4, pp. 2078–2084, Apr. 2012.

[10] J. Mahdavi, A. Emaadi, M. D. Bellar, and M. Ehsani, "Analysis of power electronic converters using the generalized state-space averaging approach," *IEEE Trans. Circuits Syst. I, Fundam. Theory Appl.*, vol. 44, no. 8, pp. 767–770, Aug. 1997.

[11] X. Liu, A. M. Cramer, and F. Pan, "Generalized average method for time-invariant modeling of inverters," *IEEE Trans. Circuits Syst. I, Reg. Papers*, vol. 64, no. 3, pp. 740–751, Mar. 2017.

[12] V. A. Caliskan, G. C. Verghese, and A. M. Stankovic, "Multi-frequency averaging of dc/dc converters," in *Proc. 5th IEEE Workshop Comput. Power Electron.*, Portland, OR, USA, 1996, pp. 113–119.

[13] C. Bernal, E. Oyarbide, P. M. Gaudo, and A. Mediano, "Dynamic model of class-E inverter with multifrequency averaged analysis," *IEEE Trans. Ind. Electron.*, vol. 59, no. 10, pp. 3737–3744, Oct. 2012.

[14] H. Behjati, L. Niu, A. Davoudi, and P. L. Chapman, "Alternative time-invariant multi-frequency modeling of PWM DC-DC converters," *IEEE Trans. Circuits Syst. I, Reg. Papers*, vol. 60, no. 11, pp. 3069–3079, Nov. 2013.

[15] J. Sun, "Characterization and performance comparison of ripple-based control for voltage regulator modules," *IEEE Trans. Power Electron.*, vol. 21, no. 2, pp. 346–353, Mar. 2006.

[16] J. W. Kimball and P. T. Krein, "Singular perturbation theory for dc-dc converters and application to PFC converters," *IEEE Trans. Power Electron.*, vol. 23, no. 6, pp. 2970–2981, Nov. 2008.

[17] B. Lehman and R. M. Bass, "Switching frequency dependent averaged models for PWM dc-dc converters," *IEEE Trans. Power Electron.*, vol. 11, no. 1, pp. 89–98, Jan. 1996.
[18] R. Tymerski and D. Li, "Extended ripple analysis of PWM dc-to-dc converters," *IEEE Trans. Power Electron.*, vol. 8, no. 4, pp. 588–595, Oct. 1993.
[19] U. Vargas, L. Renteria, A. Ramirez, and M. A. Abdel-Rahman, "Floquet domain for open-loop transient simulation of switched devices, " in *Proc. IEEE Texas Power Energy Conf.*, College Station, TX, USA, 2018, pp. 1–6.
[20] A. M. Luciano and A. G. M. Strollo, "A fast time-domain algorithm for the simulation of switching power converters," *IEEE Trans. Power Electron.*, vol. 5, no. 3, pp. 363–370, Jul. 1990.
[21] F. Guinjoan, J. Calvente, A. Poveda, and L. Martinez, "Large-signal modeling and simulation of switching dc-dc converter," *IEEE Trans. Power Electron.*, vol. 12, no. 3, pp. 485–494, May 1997.
[22] K. K. Tse, H. S. Chung, and S. Y. R. Hui, "Stepwise quadratic state-space modeling technique for simulation of power electronics circuits," *IEEE Trans. Ind. Electron.*, vol. 46, no. 1, pp. 91–99, Feb. 1999.
[23] X. Li, X. Ruan, Q. Jin, M. Sha, and C. K. Tse, "Approximate discrete-time modeling of dc-dc converters with consideration of the effects of pulse width modulation," *IEEE Trans. Power Electron.*, vol. 33, no. 8, pp. 7071–7082, Aug. 2018.
[24] M. di Bernardo and F. Vasca, "Discrete-time maps for the analysis of bifurcations and chaos in dc/dc converters," *IEEE Trans. Circuits Syst. I, Fundam. Theory Appl.*, vol. 47, no. 2, pp. 130–143, Feb. 2000.
[25] G. H. Golub and C. F. van Loan, *Matrix Computations*, 4th ed. Baltimore, MD, USA: The Johns Hopkins Univ. Press, 2013.

Yuan Chen was born in Shandong, China, in 1996. He received the B.S. degree in electrical engineering and automation in 2018 from the School of Electric Power, South China University of Technology, Guangzhou, China, where he is currently working toward the M.S. degree in electrical engineering.

His research interests include Z-source converter and modeling of power electronics converter.

Bo Zhang (Senior Member, IEEE) was born in Shanghai, China, in 1962. He received the B.S. degree in electrical engineering from Zhejiang University, Hangzhou, China, in 1982, the M.S. degree in power electronics from Southwest Jiaotong University, Chengdu, China, in 1988, and the Ph.D. degree in power electronics from the Nanjing University of Aeronautics and Astronautics, Nanjing, China, in 1994.

He is currently a Professor with the School of Electric Power, South China University of Technology, Guangzhou, China. He has authored or coauthored more than 450 papers and held 102 patents, and authored eight monographs. His research interests include nonlinear analysis and control of power electronics, wireless power transfer technology, and ac drives.

Fan Xie (Member, IEEE) received the B.S. and M.S. degrees in physics and physical electronics from the School of Physics and Electron Engineering, Guangzhou University, Guangzhou, China, in 2008 and 2011, respectively, and the Ph.D. degree in power electronics from the South China University of Technology, Guangzhou, China, in 2014.

In 2014, he joined the School of Electric Power, South China University of Technology, Guangzhou, China, where he has been an Associate Professor since 2018. His research interests include nonlinear dynamics of power electronic circuits and control of power supplies and ac drives.

Dongyuan Qiu (Member, IEEE) was born in China in 1972. She received the B.Sc. and M.Sc. degrees from the South China University of Technology, Guangzhou, China, in 1994 and 1997, respectively, and the Ph.D. degree from the City University of Hong Kong, Hong Kong, in 2002.

She is currently a Professor with the School of Electric Power, South China University of Technology. She has authored or coauthored three books and more than 200 papers and holds about 100 patents. Her main research interests include modeling of power electronic converters, wireless power transfer, and fault diagnosis.

Prof. Qiu serves as Associate Editor for the IEEE TRANSACTIONS ON POWER ELECTRONICS.

Yanfeng Chen (Member, IEEE) received the M.S. degree in power electronics technology from Wuhan University, Wuhan, China, in 1995, and the Ph.D. degree in circuits and systems from the South China University of Technology, Guangzhou, China, in 2000.

From November 2005 to December 2006, she was a Research Associate with the Department of Electronics and Information Engineering, Hong Kong Polytechnic University, Hong Kong. She is currently a Professor with the School of Electric Power, South China University of Technology. She has authored or coauthored three books, and more than 50 papers and 50 patents. Her main research interests include modeling and analysis of nonlinear systems and power electronics.